CrossMark

Geoeffective Properties of Solar Transients and Stream Interaction Regions

E.K.J. Kilpua[1] · A. Balogh[2] · R. von Steiger[3] · Y.D. Liu[4]

Abstract Interplanetary Coronal Mass Ejections (ICMEs), their possible shocks and sheaths, and co-rotating interaction regions (CIRs) are the primary large-scale heliospheric structures driving geospace disturbances at the Earth. CIRs are followed by a faster stream where Alfvénic fluctuations may drive prolonged high-latitude activity. In this paper we highlight that these structures have all different origins, solar wind conditions and as a consequence, different geomagnetic responses. We discuss general solar wind properties of sheaths, ICMEs (in particular those showing the flux rope signatures), CIRs and fast streams and how they affect their solar wind coupling efficiency and the resulting magnetospheric activity. We show that there are two different solar wind driving modes: (1) Sheath-like with turbulent magnetic fields, and large Alfvén Mach (M_A) numbers and dynamic pressure, and (2) flux rope-like with smoothly varying magnetic field direction, and lower M_A numbers and dynamic pressure. We also summarize the key properties of interplanetary shocks for space weather and how they depend on solar cycle and the driver.

✉ E.K.J. Kilpua
emilia.kilpua@helsinki.fi

Y.D. Liu
liuxying@spaceweather.ac.cn

[1] Department of Physics, University of Helsinki, Helsinki, Finland

[2] Imperial College London, London, UK

[3] International Space Science Institute, Bern, Switzerland

[4] State Key Laboratory of Space Weather, National Space Science Center, Chinese Academy of Sciences, Beijing 100190, China
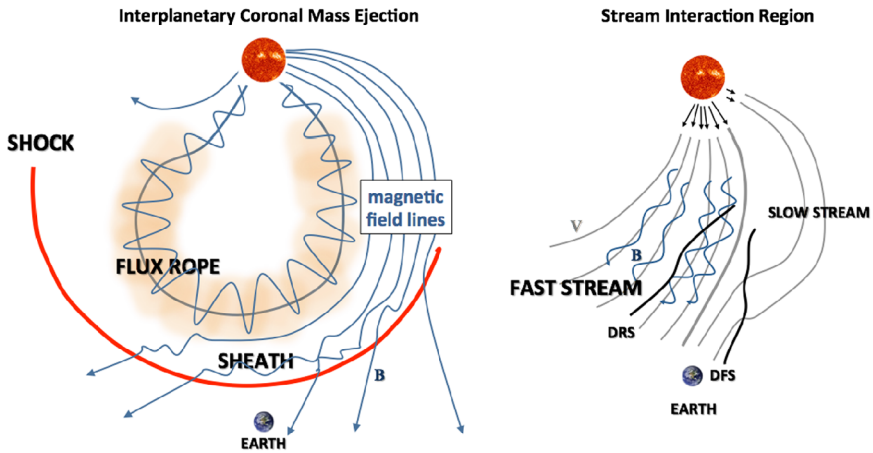
Fig. 1 Schematic of (*Left*) an Interplanetary Coronal Mass Ejection (ICME) and the associated shock (*red arc* in the figure) and sheath. The ICME shown here features the flux rope or magnetic cloud structure, see text for details. Note that not all ICMEs are fast enough to have shocks and clear sheaths. (*Right*) Co-rotating Interaction Region (CIR). Near Earth orbit CIRs are typically bounded by a developing fast forward–fast reverse shock pair (DFS and DRS)

1 Introduction

The large-scale propagating structures in interplanetary space that originate from solar wind streams and transient solar eruptions cause planetary-scale disturbances in the geomagnetic field (for a recent review, see Badruddin and Falak 2016). These magnetospheric/magnetic storms can last from hours to weeks and they are the periods when most severe space weather effects occur. During magnetic storms electric currents that flow in the magnetosphere and ionosphere, and the field-aligned currents coupling these regions are strongly intensified and relativistic electron fluxes in the Van Allen radiation belts may experience dramatic changes. Overall, geomagnetic storms are very complex phenomena, even if their typical morphology is well understood (e.g., Gonzalez et al. 1994; Pulkkinen 2007). Given their important role in space weather scenarios, they have been, and remain, extensively studied.

The most important large-scale solar wind structures that drive magnetic storms (e.g., Gosling et al. 1991; Crooker 2000; Huttunen et al. 2002; Zhang et al. 2007; Echer et al. 2008b; Richardson and Cane 2012) are shown schematically in Fig. 1. On left is an interplanetary counterpart of a coronal mass ejection (CME). CMEs are gigantic magnetized plasma clouds that are expelled on a daily basis from the Sun (e.g., Webb and Howard 2012). When detected in-situ CMEs are called interplanetary CME (ICMEs) based on a set of characteristic solar wind magnetic field, plasma and compositional signatures, see e.g., Zurbuchen and Richardson (2006) and Wimmer-Schweingruber et al. (2006). When CMEs are launched, their speed often exceeds (at least initially) the speed of the ambient solar wind ahead. Farther in the heliosphere, if the speed difference between the ICME and the preceding plasma is larger than the local magnetosonic speed a fast forward shock propagates supersonically into the upstream solar wind ahead of the ICME. Fast forward shocks are the most frequently observed shock waves in space plasmas, and also of greatest interest to space weather studies. Their impact on Earth may change dramatically the state of the magnetosphere (e.g., Samsonov et al. 2007). The ICME sheaths, i.e., the region extending from the shock to the ICME leading edge, are relatively little studied when compared to the ICME itself, but as we will demonstrate later, they are highly important drivers of space weather disturbances

(see e.g. recent review, Kilpua et al. 2017, and references therein). Sheaths pile-up gradually over several days the CME travels and expands through interplanetary space (e.g., Siscoe and Odstrcil 2008). Other key large-scale structures, Co-rotating Interaction Regions (CIRs) shown on right in Fig. 1, are compression regions that form when high-speed streams from the Sun follow and catch the slower streams ahead (e.g., Belcher and Davis 1971; Balogh et al. 1999; Gosling and Pizzo 1999). The above-discussed structures often arrive in rapid sequences or are merged together. Such interacting events can lead to particularly intense and long-lasting geospace disturbances.

Whether a given large-scale structure can drive a storm depends on its solar wind conditions. The most critical prerequisite is that the interplanetary magnetic field (IMF) is southward for a sufficiently long-time to facilitate magnetic reconnection between the interplanetary magnetic field (IMF) and the geomagnetic field (Dungey 1961; Burton et al. 1975). The rate of this reconnection is often approximated with "solar wind driving electric field", i.e., $E_Y \approx V B_S$, where V is the solar wind speed (typically very close to the Sun–Earth direction), and B_S is the southward component of the IMF (e.g., Vasyliunas 1975). In reality, solar wind—magnetospheric coupling efficiency is more complex than being a simple linear function of the driving electric field (e.g., Gonzalez et al. 1990; Pulkkinen 2007; Borovsky and Birn 2014). One of the key focuses of this review is to discuss in detail the importance of other solar wind parameters as well as the role of the Earth's magnetosheath in controlling the solar wind—magnetosphere coupling. The main focus will be on how coupling efficiency varies depending on the large-scale solar wind structure driving the storm.

The magnetosphere exhibits two basic modes or time-scales (e.g., Akasofu 1981); a directly driven mode that is related to large-scale magnetospheric convection driven by dayside reconnection and the loading-unloading mode that is related to energy storage and release process in the magnetotail, i.e., to the substorm cycle. During magnetic storms both modes are usually in action. Occasionally, periods of steady magnetospheric convection may arise when reconnection at the dayside and in the tail are balanced (e.g., Sergeev et al. 1996; Walach and Milan 2015), or alternatively, extreme substorms may occur even without sustained large-scale convection (e.g., Huttunen and Koskinen 2004; Tsurutani et al. 2015). Relevant questions related to large-scale solar wind structures and the sequences at which they arrive while interacting are also the pre-conditioning of the magnetosphere by previous activity and how long memory the system has.

Figure 2 demonstrates that the large-scale structures have clear differences in their solar wind properties. The sheath and CIR are associated with large-amplitude magnetic field fluctuations and as they are both compressed regions, they have considerably higher magnetic field and dynamic pressure than the preceding quiet solar wind. In turn, the ICME has distinctly smoother magnetic field when compared to the preceding sheath (or to CIR). The root-mean-square of the magnetic field (Fig. 2b) is clearly depressed and the magnetic field vectors rotate smoothly (Fig. 2c). These are signatures of a magnetic cloud, first introduced by Burlaga et al. (1981) as solar wind structures with (1) enhanced magnetic fields, (2) long-lasting rotation of the magnetic field direction, and (3) depressed proton temperatures. Magnetic clouds can be approximated as force-free ($\mathbf{J} \times \mathbf{B} = 0$) magnetic flux ropes (e.g., Goldstein 1983; Lepping et al. 1990). However, a significant number of ICMEs do not show clear magnetic cloud signatures due to deformation during their interplanetary journey (see Manchester et al. 2017, this issue) and/or the flux rope being sampled far from its centre (e.g., Cane et al. 1997; Liu et al. 2005; Jian et al. 2006b; Richardson and Cane 2010; Kilpua et al. 2011). The ICME in Fig. 2 drove a clear shock that is associated with an abrupt jump in the magnetic field and plasma parameters. The speed profile stays almost flat during the sheath and then declines monotonically from the leading edge of the magnetic cloud to its trailing edge. This indicates that the magnetic cloud was still expanding while it moved past
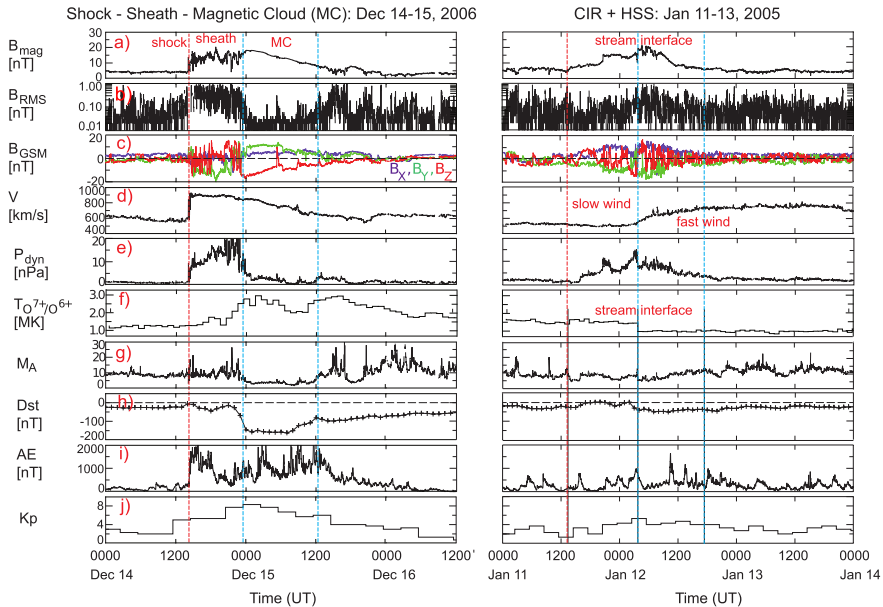
Fig. 2 Solar wind measurements and geomagnetic response during (*Left*) ICME on December 14–15, 2006 (see also a comprehensive study by Liu et al. 2008a) and (*Right*) CIR on January 11–13, 2005. The panels show from top to bottom: (**a**) magnetic field magnitude, (**b**) root-mean-square (RMS) of the magnetic field magnitude, (**c**) magnetic field components in the GSM coordinates, (**d**) solar wind speed, (**e**) Alfvén Mach number (the ratio of the solar wind speed to the Alfvén speed), (**f**) O^{7+}/O^{6+} ratio (CIR ratio is multiplied by a factor of ten), and geomagnetic indices, (**g**) Dst, (**h**) AE, and (**i**) Kp. The data (1-minute for solar wind and AE, 1-hour for Dst and Kp) is from the OMNI database. The *red dashed line* shows the ICME shock, and the magnetic cloud is bounded by a pair of *solid black lines*. In the CIR plot the *vertical lines* present in chronological order the start of the CIR, stream interface, and the end of the CIR. The times are taken from the ACE CIR catalog compiled by L. Jian

the Earth. This is a common feature of ICMEs near the orbit of the Earth (e.g., Klein and Burlaga 1982).

Within the CIR the speed increases gradually and the stream interface (e.g., Gosling et al. 1978) separates the denser and slower solar wind from the faster and more tenuous solar wind. However, due to the dynamic evolution around the stream-stream interfaces, the kinetic parameters of the solar wind (speed, density and temperature) cannot indicate equally clearly the actual stream interface between slow and fast wind (Wimmer-Schweingruber et al. 1997). The solar wind streams of different speeds and origin can be clearly separated by the oxygen ion charge state ratio (O^{7+}/O^{6+}; e.g., Geiss et al. (1995)). This transition is clearly illustrated in Fig. 2f. The charge states "freeze-in" at the distance of a few solar radii from the Sun when the propagation time of the solar wind is short compared to the recombination-ionisation time-scale (e.g., Zhao et al. 2009). At the interface between the streams, the freezing in temperature drops abruptly from 1.5 MK, corresponding to the slow wind, to ∼1 MK, corresponding to the fast wind. Note that the freezing-in temperature is high throughout the ICME in Fig. 2, showing the high coronal temperatures of the plasma, in excess of 2 MK within the magnetic cloud. Increased O^{7+}/O^{6+} ratios are known to be a good indicator of ICME-related plasma in the solar wind (e.g., Henke et al. 2001) The continued enhanced freezing-in temperature, depressed field fluctuations and low temperature (data not shown) reveal also a second much weaker ICME following shortly after the magnetic cloud.

Three bottom panels of Fig. 2 show geomagnetic activity indices Dst, AE and Kp. These indices are derived from different sets of magnetometer stations and they reflect variations in different magnetospheric and ionospheric current systems. The 1-hour Dst primarily monitors changes in the equatorial ring current, 1-minute AE is the auroral electrojet index and 3-hour Kp gives a more global activity level. Note that for Dst the more negative the index is, the large the storm. Dst values below -50 nT are generally considered as moderate storms and the intense storm threshold is -100 nT (e.g., Gonzalez et al. 1994). The NOAA Space Weather scales[1] define Kp $= 5$ as the small storm limit, and the extreme storms have the maximum possible Kp value 9. For further information of geomagnetic indices see e.g., Mayaud (1980). As the contributing current systems react differently to different solar forcing conditions and magnetospheric modes described above, there is no one-to-one correspondence between the indices (e.g., Huttunen et al. 2002; Huttunen and Koskinen 2004). In these events the sheath and the magnetic cloud both drove significant geomagnetic activity, while CIR and HSS were associated to a weaker level activity. In addition, the small ICME following the main magnetic cloud did not cause any significant response to geomagnetic indices.

The arrival of the ICME shock caused a positive excursions in Dst (panel 2g). Storm Sudden Commencements (SSCs) are precursors in the geomagnetic field of many large geomagnetic storms and indicate the first impact of a traveling disturbance on the magnetosphere (Joselyn and Tsurutani 1990). SSCs are generally associated with shocks, but they can also arise from sudden enhancements in the solar wind dynamic pressure (e.g., Wang et al. 2009; Xie et al. 2015). The lack of a shock or a clear pressure pulse preceding a geoeffective ICME or a CIR leads to a storm without an SSC, and indeed, about half of magnetic storms occur without clear SSCs (Park et al. 2015). SSCs are also associated with geomagnetically induced currents (GICs), in particular those that can occur at mid- and low-latitudes (e.g., Zhang et al. 2015). Note that Sudden Impulse (SI) refers to a case when the shock or a pressure pulse impacts on the magnetosphere, but no storm follows.
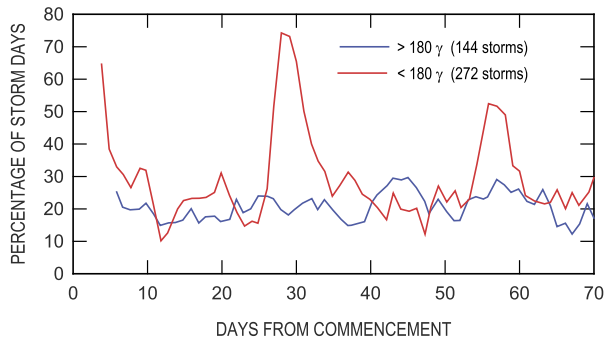
Above, we have briefly presented the main large-scale interplanetary structures that drive geomagnetic activity and highlighted the complexity of the magnetospheric response to varying solar wind driving conditions. In this review we focus in describing the space weather relevant properties of these drivers and their characteristic geomagnetic responses. We start by historical outlook on finding solar wind drivers for "recurrent" and "sporadic" geomagnetic storms in Sect. 2. In Sect. 3 we first discuss in a statistical manner solar wind properties in different large-scale structures, followed by a review on their ability to drive magnetic storms. Section 4 is focused on solar wind—magnetosphere coupling efficiency. In Sect. 5 we discuss how interactions between different large-scale drivers affect their space weather relevant parameters/properties and modify the resulting geospace response and Sect. 6 is devoted to solar cycle variations. Finally in Sect. 7 we conclude and also discuss the status and future challenges of long-lead time and near-real time space weather predictions in the context of these drivers.

2 Historical Outlook

Geomagnetic storms have been related to the Sun and solar activity for a long time. This connection was realized well before the direct physical links could be identified and the causal phenomenological chains observed, from the Sun through interplanetary space to the

---

[1]http://www.swpc.noaa.gov/noaa-scales-explanation.

magnetosphere and a plethora of terrestrial effects. The Carrington flare in 1859 and the subsequent major geomagnetic disturbance were among the first well-documented solar-terrestrial events (e.g., Carrington 1859; Cliver and Svalgaard 2004). The further works started to establish the connection between the sunspots numbers and perturbations in the geomagnetic field (e.g., Ellis 1898; Maunder 1904). Many theories of the nature of phenomena driving perturbations in the geomagnetic field emerged during the early twentieth century, but could not be explored in more detail before the space age.

Already the early studies identified two primary types of geomagnetic storms; moderate storms that have approximately 27-day recurrence and stronger and sporadic storms. In a study of 426 geomagnetic storms for the period 1874–1927, Greaves and Newton (1929) investigated the recurrence characteristics of five magnitude categories determined by the changes in declination and in the horizontal and vertical components of the geomagnetic field using Greenwich magnetic records. Figure 3 shows the recurrence characteristics for weaker and stronger storms based on this study. Weak storms (red line) are defined here those that have the horizontal or vertical geomagnetic field intensity less than 180 nT and large storms (blue line) those that have horizontal or vertical intensity exceeding 180 nT. Weaker storms have a clear recurrence signal at about 27 days, the solar synodic period, while for the two strongest categories, no recurrence was noted. For more recent study on this with similar results see, e.g., Borovsky and Denton (2006).

We now know that intense and sporadic magnetic storms are caused mostly by CMEs (e.g., Webb et al. 2000; Schwenn et al. 2005), although prior to their identification in 1970s with space-borne coronagraphs (Tousey 1973; Gosling et al. 1975), solar flares were thought to be the responsible drivers. The landmark paper by Gosling (1993) highlighted the role of CMEs in producing major transient disturbances in interplanetary space. Distinguishing the true driver was not straightforward as flares and CMEs often occur almost simultaneously and they are understood as manifestations of similar magnetic destabilization and energy release process. The early theories were indeed based on the idea that flares release "plasma clouds" or "streams of corpuscles" that propagate to the Earth and cause perturbations in the terrestrial magnetic field (e.g., Lindeman 1911; Chapman and Ferraro 1929). Plasma clouds were also suggested to explain decreases in cosmic ray intensities (e.g., Forbush 1937; Morrison 1956) and it was soon realized that such clouds should form either "magnetic tongues" of extended loops with both field lines rooted to the Sun (Cocconi et al. 1958) or "magnetic bubbles" that are completely detached from the Sun (Piddington 1958; Gold 1962). In-situ observations confirmed the existence of ICMEs soon after beginning of space era, including the likely existence of "magnetic bottles" (for the first identifications see e.g., Hirshberg et al. 1970; Gosling et al. 1973). Rapidly accumulating joint chronograph and in-situ
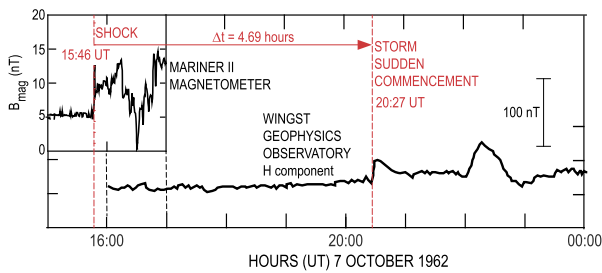
Fig. 4 The first observation of a propagating interplanetary shock wave (*inset*) by the magnetometer on Mariner II, from Sonett et al. (1964). The observation of the shock wave was followed 4.69 hours later by a Storm Sudden Commencement at Earth. The main plot shows the horizontal component of the geomagnetic field (based on Zelwer et al. 1967)

observations, e.g., by the Solwind coronagraph onboard the P78-1 spacecraft and the Helios spacecraft established a more detailed linkage between CMEs and ICMEs (e.g, Burlaga et al. 1982; Schwenn 1983; Sheeley et al. 1985).

Finding the cause for recurrent storms was not straightforward either. An explanation was put forward by Bartels (1932) who assumed that distinct regions on the Sun called M (or magnetic) regions caused the 27-day recurrence. However, no distinguishing features could be identified on the Sun, but it was noted that M-regions appeared to avoid active regions with sunspots (Allen 1944). Although the discovery of the M-regions was often claimed, and the search was slowly narrowing to the actual cause (Toman 1958; Saemundsson 1962), it was only the discovery of coronal holes with Skylab X-ray observations and associations of fast solar wind streams with them (Krieger et al. (1973) and Nolte et al. (1976), see also Cranmer (2002)) that resolved this puzzle. Coronal holes are long-lasting features on the Sun that can maintain their shape for several solar rotations. As a consequence, CIRs and related geomagnetic storms repeat on a 27-days cycles.

Another historically important phenomena related to connecting geomagnetic storms and solar wind drivers were SSC signatures in the geomagnetic field, discussed in Introduction (for definitions and history of the concepts, see e.g., Joselyn and Tsurutani 1990; Curto et al. 2007). The linkage between interplanetary shocks and SSCs was initially suggested by Gold (1955). This was before the discovery of the solar wind, the existence of interplanetary shocks and even before the main characteristics of the magnetosphere were understood. His suggestion was confirmed when the first interplanetary shock wave (Sonett et al. 1964) and the associated SSC (Zelwer et al. 1967) were identified (see Fig. 4). A strong statistical association was found between SSCs and interplanetary shocks by Chao and Lepping (1974) who studied 93 SSCs at solar maximum in 1968–1971 and found that 81 of these could be associated with solar events, although, as this was before the concept of CME was introduced, the association was with flaring activity. Of the 93 SSCs, interplanetary data were available for 48; of these 41 could be shown to be shock events. Later, over the next solar maximum between 1978 and 1981, Smith et al. (1986) found that the association between SSCs and interplanetary shocks could be unambiguously identified in about 85% of the cases.

At first, the whole concept of the interplanetary shock was puzzling. In space plasmas, contrary to hydrodynamics or even to laboratory MHD, the interaction is collisionless in the sense that the mean free paths of the particles that form the plasma are many orders of magnitude larger than the scale on which the interaction takes place. The necessary dissipation process cannot simply be located at the shock surface; it is now well known that the dissi-

pation process involves the acceleration of particles and the generation of waves that carry information about the shock far upstream into the unshocked plasma, modifying its properties that in turn affect the eventual formation of the shock wave Balogh and Riley (1997). The formation of collisionless shock waves in astrophysical plasmas is a very complex process (e.g., Treumann 2009). Phenomena at these shock waves do not meet the assumptions that would allow the application of MHD or any hydro- or gasdynamic analogy for their comprehensive description. As a consequence, the physical processes associated with the formation, structure, evolution and effects of collisionless shocks are not fully understood, even though many detailed phenomenological details have been successfully described. Basic physical considerations that have led, historically, to the definition and evolution of shock waves have been reviewed by Salas (2007).

3 Characteristic Properties and Geoeffectivity of Large-Scale Drivers

In introduction we emphasized that large-scale interplanetary structures have distinct solar wind conditions. In this section we will first study these differences statistically and then proceed on discussing the ability of different structures in driving geospace storms.

3.1 Solar Wind Conditions in Geoeffective Large-Scale Drivers

In Fig. 5 we plot the probability distributions of several space weather relevant solar wind parameters and geomagnetic indices for geoeffective (Dst at least -50 nT reached) ICMEs, sheaths, CIRs, and HSSs using the event list in Kilpua et al. (2015c). The HSS was defined as a 12-hour period following the CIR. We summarize the key features below (see also studies by Liu et al. 2006; Guo et al. 2010 and Myllys et al. 2016 that compare distributions of several solar wind parameters in sheaths and ICMEs). We note that some of the possible extreme values are excluded from the plot and as many strong events (e.g., Halloween storms in 2003) lack standard solar wind measurements.

The magnetic field distribution (panel 5a) peaks at the largest value for ICMEs, but differences are not large when compared to sheaths and CIRs, whose distributions also peak close to 10 nT. However, ICMEs and sheaths have clearly the longest strong-field tails. In turn, the HSS magnetic field distribution is clearly focused towards weaker magnetic fields; it peaks around 5 nT, which is close to the nominal solar wind value. Similar characteristics are also visible in the next panel that shows distributions for the north-south IMF component. Strongest southward fields occur predominantly in ICMEs and sheaths. The distribution of the root-mean-square of the magnetic field in Fig. 5c shows that sheaths are clearly the most turbulent of the investigated large-scale structures, followed by CIRs and then by HSSs, while ICMEs have the smoothest fields. The obvious tendency for lower fluctuation levels in ICMEs than in sheaths was shown statistically also in Kilpua et al. (2013a) where the authors conducted a superposed epoch analysis of the magnetic field fluctuation power in the Ultra Low Frequency (ULF) range.

As expected, the HSSs have on average the highest speeds, but their distribution has large variations, reflecting that not all CIRs are followed by particularly fast wind. What matters is that there is a sufficient speed gradient to form a compressive CIR. In addition, CIRs are three-dimensional structures and in some cases the spacecraft crosses only the outskirts of the CIR and may miss most of the fast stream. The speed distributions for ICMEs and sheaths peak around 400 km/s, while CIRs have the widest distribution extending to higher speeds. This is expected as the speed in CIRs generally increases gradually from the slow
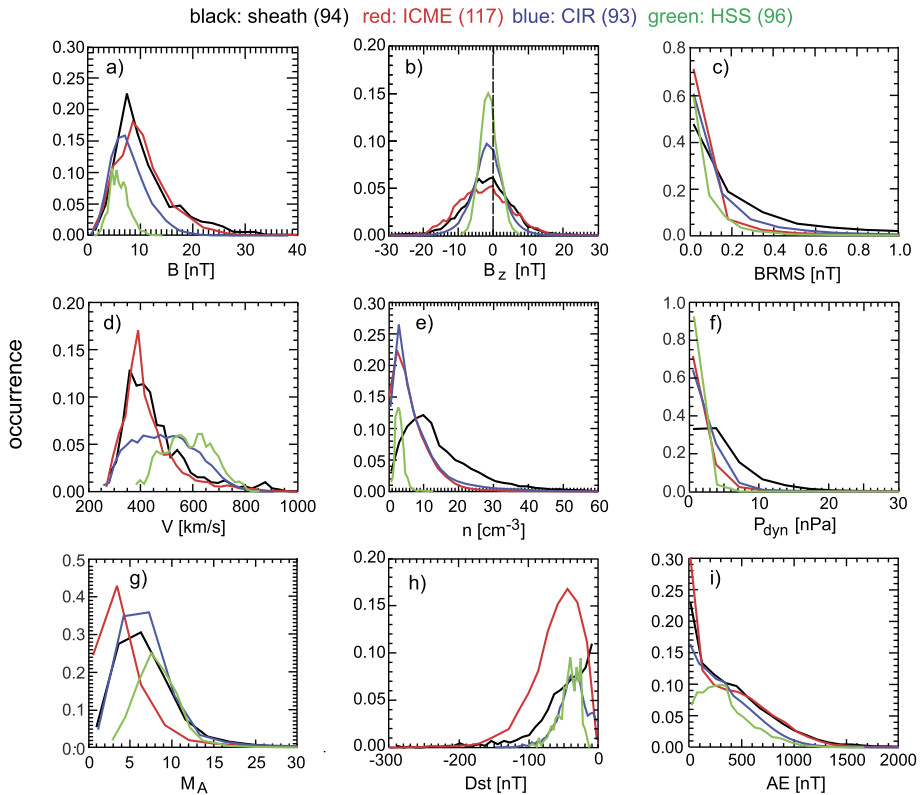
Fig. 5 Probability distributions of selected solar wind parameters and geomagnetic indices within sheaths (*black*), ICMEs (*red*), CIRs (*blue*) and HSS (*green*). To calculate the HSS distributions we used a twelve-hour interval after the CIR end time. The panels give: (**a**) magnetic field magnitude, (**b**) IMF north-south component, (**c**) root-mean-square of the magnetic field, (**d**) solar wind speed, (**e**) solar wind density, (**f**) solar dynamic pressure, (**g**) solar wind Alfvén Mach number, (**h**) Dst index, (**i**) AE index. The data are 5-minute OMNI data (Dst 1-hour). The numbers in parenthesis show the number of events in each structure category

solar wind towards the fast wind (see also Fig. 2). It should be noted that the most extreme speeds (>800 km/s) are, however, related almost solely to ICMEs and sheaths.

The next panel, density and dynamic pressure distributions, highlights that sheaths are particularly compressed regions. It is also clear from the figure that HSSs have the lowest densities and dynamic pressure of all investigated structures. The Alfvén Mach number (M_A) distributions are very similar for sheaths and CIRs. ICMEs have clear tendency towards lower M_A and it is seen that practically all of the lowest M_A conditions in the solar wind ($M_A < 4$) are related to ICMEs. The HSSs lack completely low M_A values, but their high-M_A tail matches to that of CIRs and sheaths.

3.2 Large-Scale Structures as Drivers of Magnetic Storms and High-Latitude Activity

A comprehensive survey of the different sizes of magnetic storms, as well as their solar wind origins was carried out by Richardson and Cane (2012) over four solar cycles (1963–2011). Figure 6 shows the importance of ICMEs, slow interstream solar wind, and fast streams

Fig. 6 The importance of ICMEs, slow interstream solar wind, and fast solar wind from coronal holes (including the CIRs) as drivers of geomagnetic storms over more than four full solar cycles (1964–2011). The geomagnetic storm definition shown here follows NOAA storm scale. The storm magnitude increases from small storms (G1, Kp = 5) to extreme storms (G5, Kp = 9). Figure is from Richardson and Cane (2012)
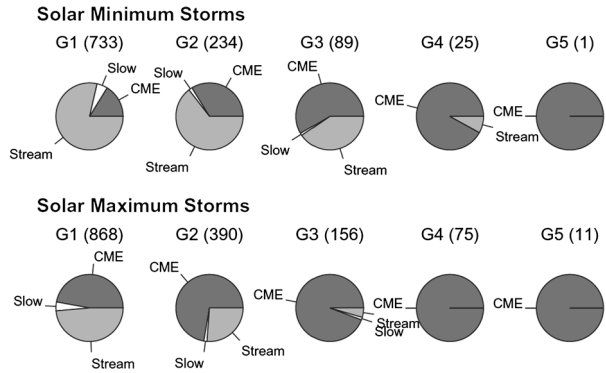
wind from coronal holes (including CIRs) as drivers of geomagnetic storms in five Kp categories following the NOAA G scale (see Introduction). We point out that in Richardson and Cane (2012) and in the papers we cite below the "storm driver" refers to the large-scale solar wind structure that had the dominant contribution in producing the peak of the geomagnetic activity (maximum Kp or minimum Dst). Note that the possible following structure(s), e.g., a CIR and HSS following an ICME, can still cause significant energy input to the magnetosphere also in the recovery phase.

Consistent with early studies discussed in Sect. 2 the pie diagrams in Fig. 6 show that ICMEs caused practically all strongest storms (G4 and G5). Although ICMEs also drive weaker and moderate storms (G1 and G2), a large fraction of them, are associated with fast streams. One reason behind this is that CIRs and HSSs are more frequently identified near the Earth, in particular during declining solar activity and at solar minimum (e.g., compare the ICME and CIR statistics published in Jian et al. 2006a and Jian et al. 2006b). The statistical analysis by Kilpua et al. (2015b) over 13 solar cycles supports the above conclusions; the occurrence of extreme storms correlates with the evolution of the toroidal magnetic field of the Sun that is connected to the formation of sunspots and active regions, where the majority of CMEs arise. In turn, the occurrence of weaker storms correlates with the evolution of the poloidal component of the Sun's magnetic field. This again emphasizes the linkage between the CIRs/HSSs and weaker storms, as poloidal field determines the distribution of coronal holes.

The Dst distributions in Fig. 5 also demonstrate that ICMEs and sheaths produced the majority of the most depressed Dst values; for Dst < −150 nT there are practically no contributions from HSSs and CIRs. These results are in agreement with the above-described Richardson and Cane (2012) study and with several other statistical studies. For example, Echer et al. (2008b) investigated the drivers of 90 intense storms (Dst < −100 nT) that occurred during Solar Cycle 23. The authors found that ICMEs were involved in the clear majority (87%) of these storms, while CIRs caused only about 13% of storms. Zhang et al. (2007) arrived to the same 13% contribution for CIRs in their investigation of the causes of 88 intense storms during 1996–2005, i.e., the period covering most of Solar Cycle 23. Nikolaeva et al. (2011) studied the effectiveness of different large-scale solar wind structures in driving 382 storms with Dst < −50 nT that occurred over multiple solar cycles (1976–2010). If we consider only those 202 storms in their study that could be clearly associated either with CIR or with an ICME, it was found that CIRs caused almost one-third (30%) of the storms. Direct comparison between different studies is not straightforward, but Nikolaeva et al. (2011) result is in agreement with Richardson and Cane (2012) and shows that the contribution from CIRs increases with decreasing storm threshold also when Dst is used
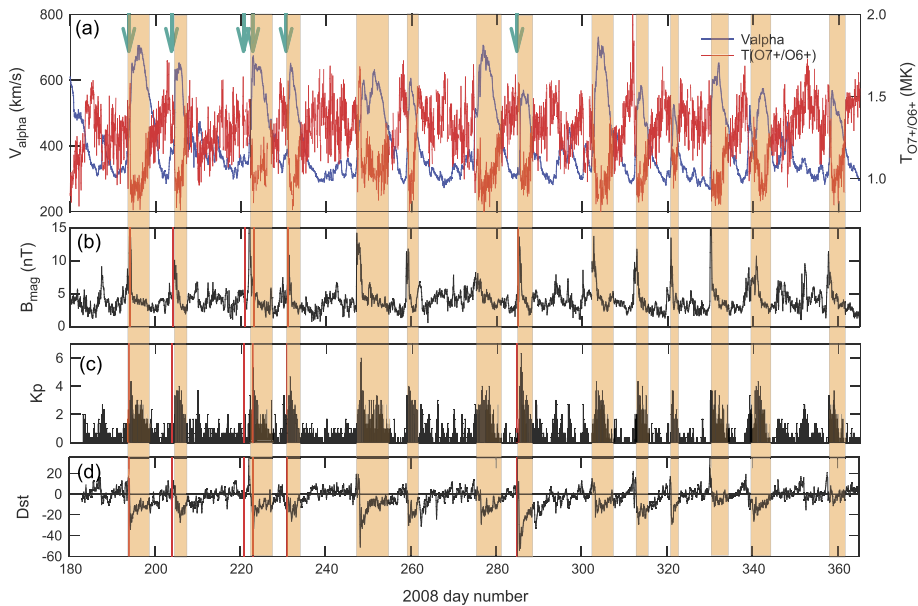
Fig. 7 A series of 14 Stream Interaction regions (SIRs) observed at 1 AU by ACE in the second half of 2008, at a time of very low solar activity, together with the signatures of their geomagnetic effects as measured by the Kp and Dst indices. Panel (**a**) shows the speed of the He^{2+} ions, equivalent to the solar wind speed (*blue line*) and the freezing-in coronal temperature (*red line*) calculated from the ratio of the Fe ions Fe^{7+}/Fe^{6+} measured by the SWICS instrument on ACE. Panel (**b**) is the magnitude of the magnetic field measured by the MAG instrument on ACE. Panels (**c**) and (**d**) show, respectively, the geomagnetic indices Kp and Dst. The *green arrows* indicate the passage of interplanetary shock waves. The *shaded areas* indicate the SIRs, identified (on this scale) by the anti-correlated (high) solar wind speed and (low) freezing-in coronal temperatures. Note that in all 14 cases, there is a corresponding geomagnetic signature, indicating low level stormy conditions

as the storm proxy. In turn, Echer et al. (2008a) found that all (11 in total) super-intense (Dst < −250 nT) storms during Solar Cycle 23 were related to ICMEs and sheaths, i.e., none of them were driven by a CIR. Although ICMEs and their sheaths clearly dominate as causes of intense geomagnetic storms, we note that CIRs and HSS have an important role in enhancing the geoeffectivity of some ICMEs (Sect. 5) and in prolonging the recovery phase of the storm (see below).

The geomagnetic effects of CIRs are further illustrated in Fig. 7, showing a series of 14 CIRs in the second half of 2008, observed at 1 AU by the ACE spacecraft. The CIRs were identified by the presence of HSSs, preceded by a compression in the magnetic field. The sudden drop in the freezing-in temperature at the leading edges of the HSSs indicates the stream interfaces. Note that only five of the CIRs were preceded by a shock wave, the others had not steepened enough to form a shock at 1 AU. All shown 14 CIRs were accompanied by a recognizable geomagnetic signature, but usually the minimum of the Dst did not exceed the moderate storm limit (Dst < −50 nT). For most of the cases the Kp index reached 3+ to 4+, i.e., the NOAA scale small storm limit (Kp = 5) was not exceeded. The likelihood of CIRs/HSSs in driving moderate storms increases in the declining phase, as we will discuss in Sect. 6.1.

As sheaths and ICMEs have different origin and solar wind conditions, it is also important to investigate their separated contributions as storm drivers. Now we consider only the subset

of storms that can be traced to an eruption of a CME at the Sun. In Echer et al. (2008b) study 47% of such intense storms were caused by ICMEs, 31% were pure sheath storms, and 22% had contribution both from the sheath and ICME. Zhang et al. (2007) found that 69% of storms were ICMEs-driven, and 31% were sheath-driven. Nikolaeva et al. (2011) arrived to very similar percentages for CME induced moderate storms. In their study 68% of Dst < −50 nT storms were associated to ICMEs, and 32% to sheaths. Note that Nikolaeva et al. (2011) and Zhang et al. (2007) did not report the percentage of the events with significant contribution from both the sheath and ICME.

Some studies however highlight the role of sheaths as storm drivers. One of the earliest statistical studies that demonstrated the relevance of sheath fields was conducted by Tsurutani et al. (1988). The authors showed that for 10 storms that occurred near Solar Cycle 21 maximum the sheaths had equal importance to ICMEs. A statistical analysis by Huttunen et al. (2002) found that in 1996–1999 two-third of intense storms when defined by Kp were either pure sheath storms or the sheath had a big influence. When Dst was used as the proxy of the geomagnetic activity the importance of ICMEs as storm drivers increased. When the analysis was extended to cover Solar Cycle 23 maximum by Huttunen and Koskinen (2004) sheaths drove the largest fraction also of intense Dst storms. As we will discuss in Sect. 6.1, the relative importance of different structures as storm drivers varies with solar activity cycle.

Differences between large-scale structures as drivers of auroral activity and substorms is less systematically studied. Auroral region activity can be studied using geomagnetic indices (e.g., AE, AL and AU, see Mayaud 1980) that are derived from high-latitude magnetometer stations. Substorms manifest themselves with various signatures from which one of the clearest one are is the rapid injections of energetic charged particles to geosynchronous orbit when the geomagnetic tail reconfigures (e.g., Koskinen 2011 and references therein). These injections are followed by slow decay and when they occur at about 2–4 periodicity they are called as sawtooth oscillations. These oscillations occur both during fluctuating and smooth IMF and roughly with the same periodicity (Huang et al. 2004). However, Brambles et al. (2013) found the evidence using a global multi-fluid simulation that sawtooth events during CIRs are externally triggered, while ICME related sawtooths are internally triggered. Farrugia et al. (1993) studied the substorm activity during ∼18 hours of southward IMF associated with the MC passage. The authors identified over 20 substorms during this interval that repeated with a rapid 50 min periodicity, even when solar wind driving diminished due to decreasing magnetic field magnitude and solar wind speed in the end part of the MC. This occurrence frequency agrees with the model developed by Klimas et al. (1992), but is substantially shorter than 2–3 hours reported in several other studies (e.g., Borovsky et al. 1993; Baker et al. 1991; Huang et al. 2004; Borovsky and Yakymenko 2017). As pointed out by Huang et al. (2004), at some periods resonant state of the magnetosphere may exist where solar wind oscillations are comparable with the substorm cycle. Too fast oscillations prevent enough energy to accumulated and if oscillations are too long the energy will be released through internally triggered processes.

Statistical studies show that substorms induced by ICMEs are on average stronger and they occur at lower geomagnetic latitudes than substorms related to CIRs and HSSs (e.g., Holappa et al. 2014; Myllys et al. 2015). Huttunen and Koskinen (2004) showed that sheaths and CIRs can cause considerable high-latitude activity and strong substorms even though the ring current is not significantly enhanced. Similarly, in Nikolaeva et al. (2011) study sheaths were associated with the largest average AE values for a given solar wind electric field than ICMEs and CIRs.

If one considers cumulative effects rather than more instantaneous strong high-latitude activity, the role of HSSs is emphasized. Tsurutani et al. (2006) remarked that recovery

phases of CIR-storms can extend up to 27 days. This is attributed to Alfvénic fluctuations in the following HSSs (e.g., Tsurutani and Gonzalez 1987; Balogh et al. 1995; Tsurutani et al. 1995; Lucek and Balogh 1998) that ultimately originate from the Sun and propagate along open field lines into the heliosphere (e.g., Tomczyk and McIntosh 2009). Combined with high solar wind speed these Alfvénic fluctuations cause intermittent but prolonged dayside reconnection that drives efficiently high-latitude geomagnetic activity, called also as High-Intensity, Long-Duration, Continuous AE Activity (HILDCAA) (Tsurutani and Gonzalez 1987). Tanskanen et al. (2005) further showed that during the years when HSSs were frequent substorms deposited approximately twice as much magnetic energy to the auroral ionosphere than during those years when only few HSSs occurred.

3.2.1 ICMEs and Magnetic Clouds

Not all ICMEs are equally geoeffective. Some of them drive extreme storms, while the others pass the Earth practically unnoticed. Near the Earth orbit ICME speeds vary from typical slow solar wind speeds up to few thousands kilometers per second and their magnetic fields range from only a few nT to up about 100 nT. What we observe in-situ is determined by intrinsic CME properties, the evolution and interaction of the CME with the ambient solar wind (see Manchester et al. 2017, this issue, and the references therein), and the path the observing spacecraft (and the Earth) makes through the ICME.

Table 1 shows the Dst response of ICMEs based on their magnetic complexity. The events shown are taken from the Richardson and Cane ICME list[2] and they are divided to MCs, non-MCs and MC-like events. MC-like events show rotation of the field, but they lack other specific MC signatures. Table 1 clearly shows that MCs are the most geoeffective subset of ICMEs. They are associated with clearly stronger average Dst disturbance than non-MCs and MC-like events and a higher fraction of them caused moderate and intense storms. This result is expected as the lack of clear MC signature in ICMEs is generally attributed to cases where the spacecraft crosses the flux rope farther from the centre where the field is typically weaker (see Introduction). Non-MC events likely represent interacting ICMEs, so called complex ejecta (see Sect. 5), where individual MC characteristics are lost. Note that in Table 1 the sheath and MC contributions have not been separated, i.e., part of the storms may have been driven by the sheath alone or the sheath had a significant contribution. However, whatever the geoeffective structure is, the results show that ICMEs that contain MCs are clearly the most likely to drive significant geomagnetic activity.

The results shown in Table 1 are also consistent with statistical studies we discussed in Sect. 3.2. In Zhang et al. (2007) study from those 41 intense storms in their study that were driven by ICMEs, 30 (73%) were MCs. Nikolaeva et al. (2011) also showed that non-MC ICMEs and CIRs were associated with clearly lower average electric fields and geomagnetic responses than the other investigated structures, emphasising again that MCs are associated with stronger geomagnetic activity than non-MC ICMEs and CIRs.

The strong potential of MCs to drive magnetic storms stems from their enhanced magnetic fields and smooth field rotation creating particular favorable conditions for long-lasting and strong magnetospheric convection. Several studies have also indicated a clear relationship between the speed of an MC and its magnetic field (e.g., Gonzalez et al. 1998; Owens et al. 2005; Richardson and Cane 2010), i.e., stronger MCs tend to be faster, which enhances their geoeffectivity. According to Gonzalez and Tsurutani (1987) intense magnetic storms (Dst < -100 nT) require that the solar wind driving electric field E_Y is equal or larger than

---

[2]http://www.srl.caltech.edu/ACE/ASC/DATA/level3/icmetable2.htm.

Table 1 The geoeffectivity of magnetic clouds (MC), cloud-like events (MC-like) and non-magnetic cloud (non-MC) ICMEs. MC-like events have at least weak rotation in the field, but they lack other MC characteristics. The events and Dst values are taken from the Richardson and Cane online ICME catalog for the period from 1995 to 2016. The first column (N) gives the number of events in each driver category and the second column ($<$ Dst $>$) shows the averages of the resulting storm Dst minima. The last two columns show the percentages of events (number of such events in parenthesis) in each driver category that caused Dst < -100 nT and Dst < -200 nT storms

	N	⟨Dst⟩	Dst < -100 nT	Dst < -200 nT
MC	170	-86.7	34% (57)	7% (12)
MC-like	161	-51.8	11% (17)	4% (6)
non-MC	147	-41.6	11% (16)	1% (2)

5 mV/m at least for 3 hours. As MCs have on average strong magnetic fields, also slow MCs can create large enough electric fields to drive intense magnetic storms (Tsurutani et al. 2004).

The geomagnetic response of a given MC depends also strongly on its flux rope type (e.g., Huttunen et al. 2005), i.e., how the IMF B_Z rotates within the cloud (e.g., Bothmer and Schwenn 1998; Mulligan et al. 1998). In bipolar MCs the field rotates either from north to south (SN) or south to north (SN), see Fig. 2 for an example of an SN-type MC. Such clouds are also called low-inclination as their axes are more or less aligned with respect to the ecliptic plane. In turn in unipolar or high-inclination MCs (N- and S-type) the field rotates in a way that B_Z maintains its sign.

It is clear that MCs with fully northward fields (i.e., N-type MCs) cannot drive magnetic storms, while MCs with fully southward fields (S-type MCs) provide the most long-lasting southward IMF and they typically drive intense storms. Figure 8 shows examples of both S-type and N-type MCs and their geomagnetic responses. The unipolar S-type MC on 19–20 November, 2003, shown on left in Fig. 8, drove the largest Dst storm of Solar Cycle 23 (-422 nT). In turn, although the sheath of the N-type MC shown on right caused some substorm activity (enhanced AE and Kp values), the MC itself did not cause any significant geomagnetic activity. In particular the AE index shows that the activity in the auroral region was minimal during the whole passage of the MC.

N-type MCs may also lead to false space weather alerts. Even if a CME would be fast and associated with a strong flare, no storm follows if its magnetic field in the MC is northward. One interesting example of such a case was the CME on August 1972 that was associated to a major flare and that had one of the fastest Sun-to-Earth transit times ever reported (Tsurutani et al. 1992), but no significant geomagnetic activity followed due to northward fields.

Bipolar/low-inclination MCs have also distinct differences in their geospace responses (e.g., Kilpua et al. 2012). For example, the expansion of the CME can attenuate significantly the geoeffectivity of an NS type cloud as the magnetic field and speed are weaker in the trailing part of the cloud where the field is directed southward. In turn, compression of the tail part by a fast stream can enhance significantly geomagnetic response of an NS-type MC (discussed in more detail in Sect. 5).

3.2.2 Shocks and Sheath Regions

As discussed in Sect. 3.2 ICME sheaths are important drivers of magnetic storms and their importance increases when high-latitude activity is considered. It is also interesting to note
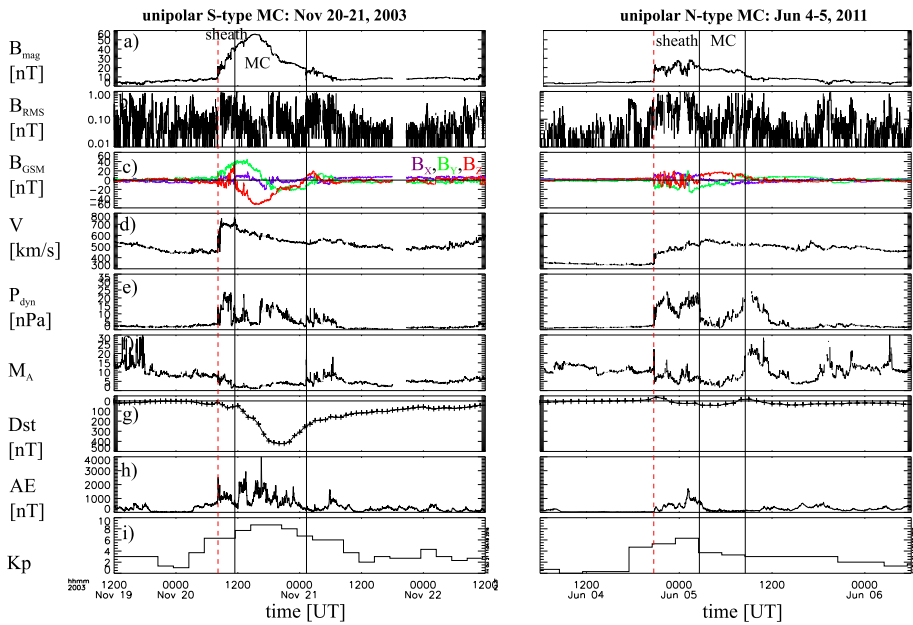
Fig. 8 Unipolar magnetic clouds (MCs) observed in the near-Earth solar wind. (*Left*) S-type MC observed on November 20–21, 2003. (*Right*) N-type MC observed on June 4–5, 2011. The panels are the same as in Fig. 2. The *dashed line* indicates the fast forward shock and the pair of *solid lines* bound the MC
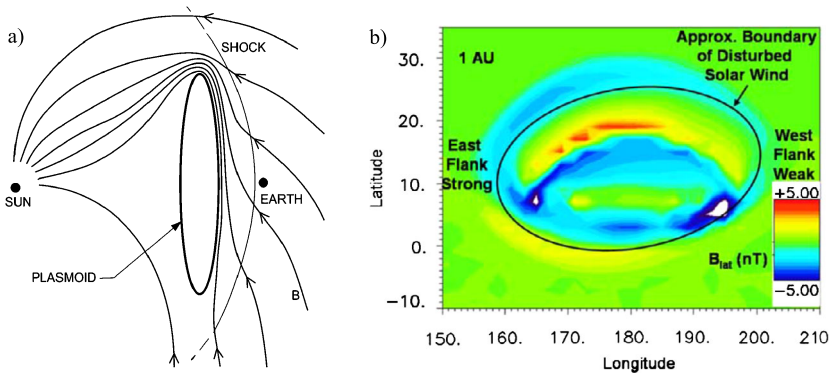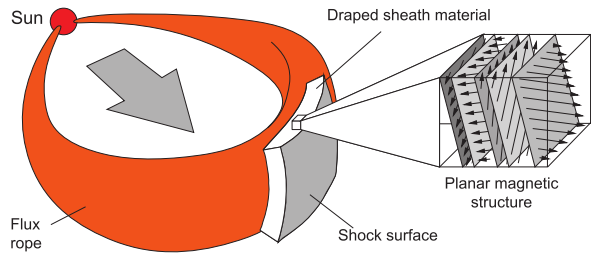

Fig. 9 Direction of the out-of-ecliptic fields in CME sheaths (**a**) for radial IMF from Gosling and McComas (1987). Note that this is a meridional cut, (**b**) Parker spiral-type solar wind from the global MHD simulation by (Siscoe et al. 2007). The strength of the out-of-ecliptic IMF component is shown for a view towards the Sun. The relevant part to focus here are the outer boundary and outskirts of the ellipse that corresponds to the ejecta

that Nikolaeva et al. (2011) showed that on average, sheath regions preceding MCs (only eight included for the whole data set) were associated clearly to the largest driving electric fields and strongest storms and substorms from all investigated driver categories.

There are two basic mechanisms that create strong southward magnetic fields in sheaths (e.g., Gonzalez et al. 1994; Kataoka et al. 2005; Liu et al. 2008b): (1) processes related to the

Fig. 10 Formation of planar magnetic structures in an ICME sheath. Figure is from Jones et al. (2002)

shock transition, i.e., the compression of the pre-existing southward IMF and the deflection of the IMF, and (2) draping of the IMF around the CME.

Figure 9 shows how the direction of the out-of-ecliptic magnetic fields in the sheath depends on the upstream field direction and the CME propagation direction. Panel (a) is from Gosling and McComas (1987) for the radial IMF. According to their "Bz forecasting rule" geoeffective sheaths occur when the IMF points away (towards) the Sun and the CME passes southward (northward) of the Earth. The applicability of this technique to predict the dominant sign of B_Z in ICME sheaths was tested by McComas et al. (1989) for 17 fast ICMEs. The authors found that the rule predicted correctly the sign of the B_Z perturbation for 13 events (76%). It was however noted that from the initial set of 26 fast ICMEs nine did not exhibit clear change in the average B_Z upstream of the shock to the ICME leading edge, hence decreasing the amount of events for which this technique can be applied. The Gosling and McComas (1987) scenario was extended by Siscoe et al. (2007) to take into account the Parker spiral type configuration. The results from their global MHD simulation are shown in Fig. 9b. The plot shows that the strongest out-of-ecliptic magnetic fields are found at the eastern flank of the CMEs (the area outside the ellipse that corresponds the ICME). This implies that the eastern flank of the ICME would be more geoeffective, and as suggested by the authors, could explain the known greater geoeffectiveness of CMEs originating from the western hemisphere (e.g., Wang et al. 2002). The magnetic field variations related to shock processes and draping effects occur typically parallel to a single plane called as "planar magnetic structures" (e.g., Jones and Balogh 2000; Jones et al. 2002; Palmerio et al. 2016) (see Fig. 10). Palmerio et al. (2016) showed that the planar parts of the sheath are associated with considerably larger out-of-ecliptic fields than non-planar parts, and are, hence, expected to be the most geoeffective.

The shock angle (i.e., the angle between the shock normal and the upstream magnetic field) has a big influence on how geoeffective the following structure will be. For example, Jurac et al. (2002) studied 107 fast forward shocks observed by Wind in the near-Earth solar wind. The authors showed that regardless of the shock driver 40% of quasi-perpendicular fast forward shocks were associated with an intense storm within 48 hours from the shock passage compared to only 10–15% for quasi-parallel shocks. Quasi-perpendicular and -parallel shocks have different internal structure, because the shock angle (θ_{Bn}) controls the behavior of the particles incident to the shock. Quasi-parallel shocks feature an extended foreshock and wave activity, and as a consequence, the shock transition is more gradual than at quasi-perpendicular shocks (e.g., Bale et al. 2005; Burgess et al. 2005; Lucek et al. 2008; Kilpua et al. 2015a). Examples of quasi-perpendicular and parallel shocks are shown in Fig. 11.

In addition, the shock impact angle (i.e., the angle between the shock normal and the Sun–Earth line) affects the geomagnetic response. Frontal shock collisions compress the whole magnetosphere symmetrically, while inclined collisions lead to an asymmetric collision (e.g., Samsonov et al. 2015). According to global MHD simulations performed by
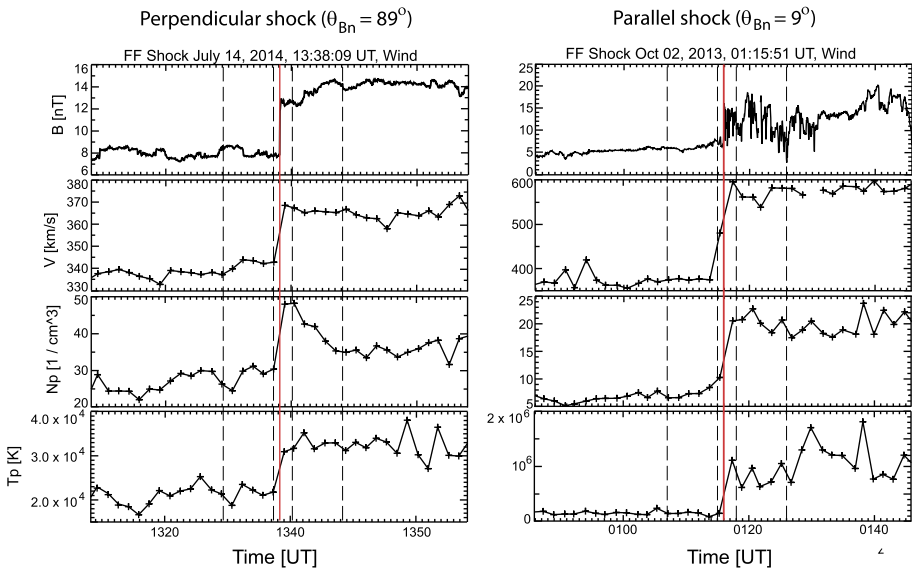
Fig. 11 Examples of (*Left*) quasi-perpendicular and (*Right*) quasi-parallel shocks detected by Wind. The shocks are from the Heliospheric Shock Database (ipshocks.fi)

Oliveira and Raeder (2014) inclined shocks are associated to overall weaker compression of the magnetosphere and weaker response of the field-aligned currents coupling the magnetosphere and ionosphere than head-on shock impacts. The authors also reported that despite otherwise similar parameters the head-on case in their study triggered a substorm, while the inclined shock did not. The stronger auroral response for frontal shocks was also evident in the extensive experimental study by Oliveira and Raeder (2015) where the authors used the geomagnetic index derived from more than 300 SuperMAG magnetometer stations. The authors suggest that symmetric compression of the magnetosphere associated with frontal shocks creates favorable conditions for the release of magnetic energy stored in the magnetotail. We note that CIRs are generally associated with larger impact angle, i.e., being more inclined than ICME-driven shocks (e.g., Jurac et al. 2002; Kilpua et al. 2015a).

Figure 12 in turn features an exceptional shock wave observed by the STEREO-A spacecraft on 23 July 2012 (Liu et al. 2014a). Riley et al. (2016) determined that the shock was quasi-parallel, with an extremely high speed of 3300 km/s, reaching STEREO-A (0.96 AU) in 18.6 hours, and unusually high sonic Mach number ($M_S = 28$), and that the shock normal was pointing very close to the radial direction. They also concluded that what was observed by STEREO-A was the result of the interaction of two exceptional CMEs, propagating into interplanetary space that had been pre-conditioned by a previous CME, so as to influence significantly the formation, evolution and propagation of the shock wave and the CME ejecta. The observed event was thus caused by compound and exceptional conditions, both in the corona and in interplanetary space. Given the extraordinary parameter regime of the event, the STEREO-A plasma instruments could not make all the measurements that would have been necessary for a full description of the observations. Russell et al. (2013) noted that this shock actually rather resembled a subsonically driven compressional disturbance due to intense flux of very high energy particles related to the strong CME. The authors also argued that this could have likely weakened the shock-related space weather consequences. As was concluded by Riley et al. (2016), it remains unclear what role high

Fig. 12 The exceptional shock wave observed by the STEREO-A spacecraft on 23 July 2012. The panels show (**a**) the magnetic field magnitude, (**b**) the magnetic field normal component, solar wind (**c**) speed and (**d**) density, and (**e**) simulated Dst index. Because of the difficulties of processing the data from the plasma instrument due to the exceptional speeds, densities and temperatures this plot is a composite reconstruction of the best available data (see Liu et al. 2014a)
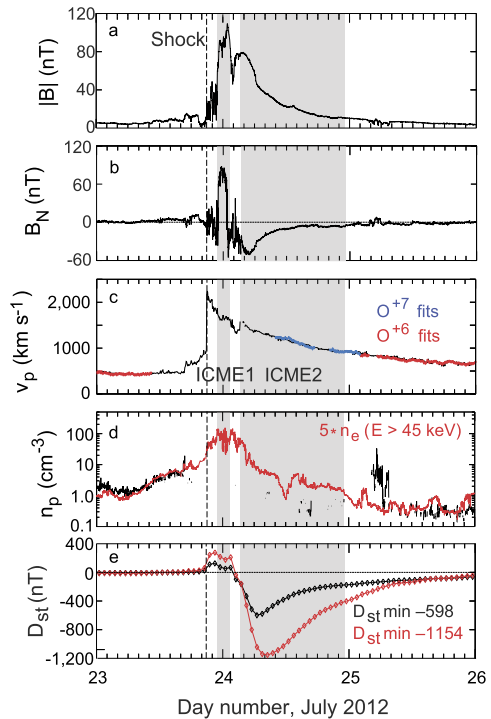

energy particles played in the observations. This exceptional shock wave illustrates the potentially extreme events that can be caused by CMEs, with a major impact on a large region of the inner heliosphere and, if Earth-directed, causing extreme disturbances in the near-Earth space as well as on the ground.

3.2.3 CIRs and High-Speed Streams

Similarly to ICMEs not all CIRs that pass the Earth are geoeffective. Alves et al. (2006) showed that approximately one-third of CIRs during 1964–2003 were followed by at least a moderate (Dst < -50 nT) magnetic storm. The leading shock enhances the ability of a CIR to drive a storm; according to Zhang et al. (2008) a clear majority (85%) of shock-driving CIRs produced a storm.

The evolution of a CIR structure at the Earth orbit at three spacecraft is shown in Fig. 13: ACE sunward of the Earth at L1, STEREO-A and B, close to 1 AU, but to the west and the east of the Sun–Earth line by about 23°, respectively (see the orbits on the left hand side in Fig. 13). The front of this corotating structure was observed first at STEREO-B, then at the Earth (as observed by ACE), followed by STEREO-A. At STEREO-B there is no evidence of a shock forming (although the solar wind velocity increases sharply) and there is an increase in the magnetic field magnitude, indicating the compression. At ACE, the magnetic field has already steepened considerably, ready to form the forward shock. At STEREO-A, both forward and reverse shocks were identified. As the evolution of this CIR structure varies in longitude, at least at 1 AU the geoeffectivity of a CIR may vary in longitude in the interplanetary space. Panel (d) in Fig. 13 shows the oxygen freezing-in temperature at ACE clearly identifying the stream interface between the slow and fast wind
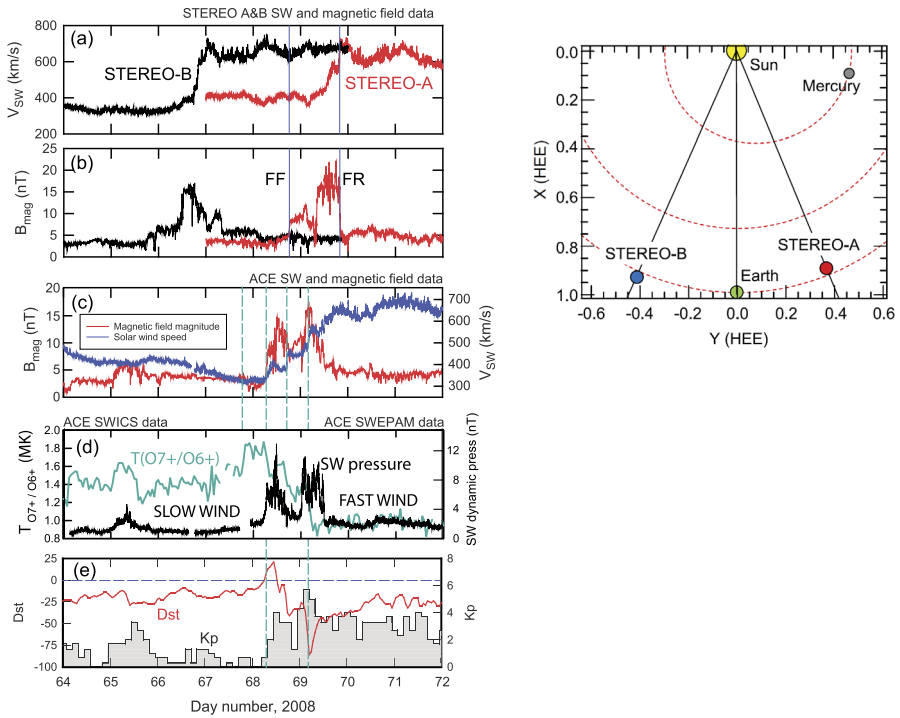
Fig. 13 (*Left*) The evolution of a CIR near 1 AU as seen by STEREO-B, ACE and STEREO-A. Te panels show: (**a**)–(**b**) the solar wind speed and magnetic field magnitude at the two STEREO spacecraft, respectively, (**c**) the magnetic field and solar wind speed profiles observed at 1 AU by ACE, (**d**) oxygen freezing-in temperature measured at ACE, (*black line*). In addition, panel (**e**) shows the geomagnetic response to the CIR, in terms of the disturbance indices Dst and Kp. (*Right*) The positions of the three spacecraft that observed the CIR are shown on 8 March 2008

streams, not so clearly seen in the kinetic parameters of the solar wind. The oxygen freezing-in temperature profile shows that in this case the slow wind ahead of the interaction region was a compound stream, corroborated by the solar wind dynamic pressure. Even though the compression within CIR at ACE was (apparently) not enough to form either a forward or a reverse shock, the solar wind pressure increase was sufficient to trigger a moderate geomagnetic storm, with Dst = −85 nT and a maximum Kp = 6. A search of geomagnetic data records for the time did not show the occurrence of a SSC, confirming that the CIR leading edge had not formed a shock wave.

Figure 14 shows the close-up the magnetic field measurements for the CIR shocks in Fig. 13 as detected by STEREO-A. The panels show the 32 Hz and 8 Hz magnetic field data in the left and right panels, respectively, for the forward and reverse shocks, over equal, 60 seconds, intervals. The left panels in Fig. 14 illustrate the very prominent wave field in the upstream region, known to be whistler waves generated at the shock. In the right panels the data show clearly how the waves decay when moving away from the shock in the upstream region. The downstream waves in the left hand panel are likely to be magnetosonic waves (Russell et al. 2009). An overview of the generally low Mach number shock waves and the waves associated with both the upstream and downstream regions, as observed by the STEREO mission, was given by (Blanco-Cano et al. 2016).
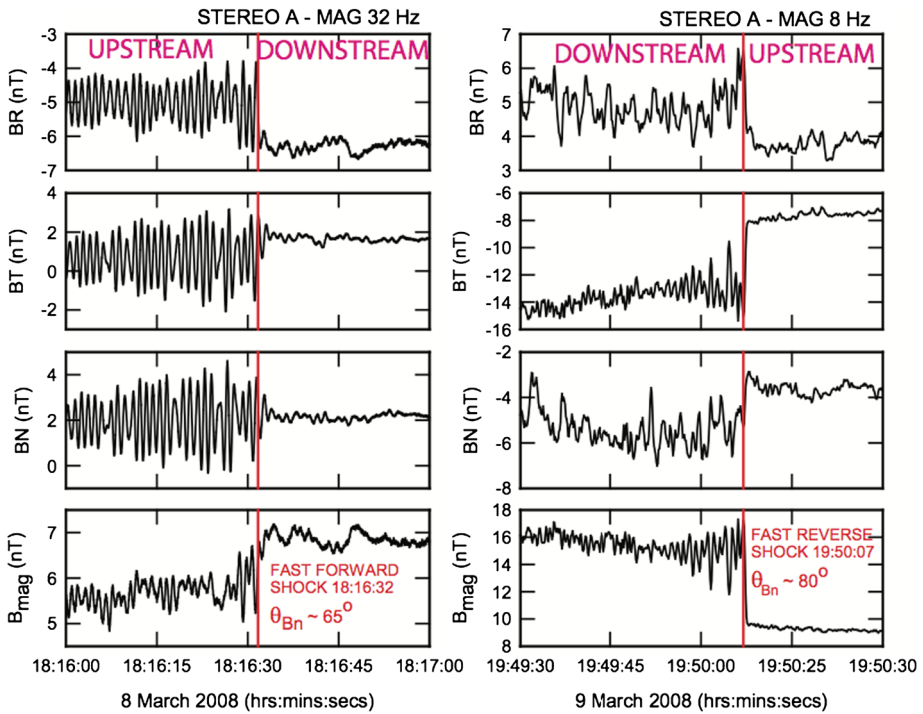
Fig. 14 A close-up of the shock shown in Fig. 13 at STEREO-A. The panels show (**a**)–(**c**) the magnetic field components in the RTN system, (**d**) the magnetic field magnitude. In the *left panels* the frequency of the measurements in 32 Hz and in the *right panels* 8 Hz

The most geoeffective part of a CIR is the region after the stream interface. The super-posed epoch analysis using multiple epoch times by Kilpua et al. (2015c) showed that this part has strongest southward fields, speed and magnetic field fluctuation levels. For CIRs that were followed by slower streams the activity declined soon after the interface, while for CIRs that were followed by fast streams the activity continued at relatively high-levels until the end of the CIR and then declined slowly during the following HSS. Considering the effects of the HSS, the Alfvénicity is a critical parameter for causing prolonged geomagnetic activity (see discussion in Sect. 3.2). Snekvik et al. (2013) showed that HSSs with strong Alfvénicity are the most geoeffective as such streams tend to have clearly higher speeds and magnetic fields and slightly higher dynamic pressure than mostly non-Alfvénic streams.

It is also clear that CIRs that embed ICMEs are generally more geoeffective than "pure" CIRs. For example, Zhang et al. (2008) found that from 345 CIRs identified during Solar Cycle 23 157 were "pure" CIRs and they caused mainly weak and moderate storms, while CIRs with ICMEs could drive significantly stronger responses (see Sect. 5). Many CIRs also embed small ICME-like transients, i.e., solar wind periods that feature many ICME signatures, such as smooth/coherent field rotation and enhanced fields, but that are significantly shorter in duration (a few hours on average) than typical large-scale ICMEs (e.g., Moldwin et al. 2000; Kilpua et al. 2009; Yu et al. 2014). Entrainment of such transients, when they have southward fields, may enhance the geoeffectiveness of a CIR. The origin of these transients is not clear, but at least part of them are associated to streamer blobs (e.g., Sheeley and Rouillard 2010; Rouillard et al. 2011) that are released in quasi-continuous manner, likely

via magnetic reconnection, from the Sun (e.g., Sheeley et al. 1997). More studies are needed to clarify how these blobs modify the global CIR structures and their geoeffectiveness.

CIRs can be associated either with helmet streamers or pseudo-streamers (e.g., Crooker et al. 2012). Helmet streamers are loop structures that separate two coronal holes of the same polarity, while pseudo-streamers separate coronal holes of the same polarity (Wang et al. 2007). Borovsky and Denton (2013) showed that although storms associated with helmet streamer CIRs and pseudo streamer CIRs have similar overall magnitudes, they feature some obvious differences in their characteristics (see their Table 1). The most significant differences are that helmet streamer CIRs have higher densities and dynamic pressure than pseudo-streamer CIRs that also tend to peak earlier concomitant with the magnetic field, and clearly longer duration HSS following them. In addition, the authors emphasized that the helmet streamer CIRs are often preceded by "a calm before the storm", i.e., a particularly low geomagnetic activity period that pre-conditions the magnetosphere by building-up the plasmasphere and the plasma sheet. This is because the helmet streamer CIRs tend to have considerably lower solar wind speed, density and dynamic pressure preceding them than the pseudo-streamer CIRs. Interesting questions are also whether the above-discussed streamer blobs occur from pseudo-streamers and whether they have similar frequencies and properties as the blobs emanating from helmet streamers.

4 Solar Wind Magnetosphere Coupling Efficiency During Large-Scale Drivers

In this section we discuss the current knowledge on how the solar wind—magnetosphere coupling efficiency depends on different solar wind parameters and the type of the associated large-scale driver.

4.1 Definition of the Coupling Efficiency

The solar wind—magnetosphere coupling efficiency is defined as the ratio of the input to output energies. One of the simplest energy input estimate, or the so-called "coupling function", is the solar wind driving electric field E_Y. As we mentioned in Introduction, the true coupling efficiency is however more complex. Over the years several coupling functions have been developed, such as the widely used epsilon parameter (e.g., Akasofu 1979, 1981; Koskinen and Tanskanen 2002). For a comprehensive review of early coupling functions see Gonzalez et al. (1990). Examples of more recent coupling functions are the ones formulated by Newell et al. (2007) and Borovsky (2008). The energy consumed in the ring current and in the ionosphere as Joule heating and via auroral precipitation can be estimated in terms of geomagnetic indices (e.g., Yermolaev et al. 2010; Myllys et al. 2016) or functions based on them (Ahn et al. 1983; Knipp et al. 2004), using global numerical simulations (e.g., Palmroth et al. 2004), or if available, using actual satellite measurements (e.g., Turner et al. 2006).

The studies comparing coupling efficiency for different storm drivers (e.g., Turner et al. 2009; Yermolaev et al. 2010; Myllys et al. 2016) show that ICMEs, despite being the key drivers of intense geomagnetic storms, have on average the weakest coupling efficiency. This can be traced to their characteristic plasma and magnetic field conditions we highlighted in Sect. 3.1.

4.2 Influence of Various Solar Wind Parameters

The solar wind Alfvén Mach number (M_A; i.e., the ratio of the solar wind speed to the Alfvén speed), is particularly important parameter for controlling the coupling efficiency. Firstly, M_A controls how efficiently the plasma and magnetic field are compressed at the bow shock (Lopez et al. 2004). The larger the Alfvén Mach number is, the more compression at the bow shock occurs. The tendency for low M_A in ICMEs when compared to sheaths and CIRs should therefore lead to weaker bow shock and weaker compression of the plasma and magnetic field (e.g., Turc et al. 2015; Lugaz et al. 2016). The Alfvén Mach number has also an important role in controlling the saturation of the polar cap potential. The saturation means that although the solar wind driving electric field E_Y would intensify, the magnetosphere cannot dissipate energy more effectively. Saturation generally occurs during intense solar wind driving (e.g., Reiff et al. 1981; Hairston et al. 2005; Raeder and Lu 2005), but when M_A is low the saturation can occur even during the moderate driving conditions (e.g., Lavraud and Borovsky 2008; Lopez et al. 2010; Myllys et al. 2016). These results imply that during ICMEs saturation may occur already during relatively low solar wind driving when compared to sheaths an CIRs.

Another important effect attributed to low Alfvén Mach number solar wind conditions is the resulting low plasma beta in the magnetosheath (e.g., Lavraud and Borovsky 2008). Based on this Lopez et al. (2010) presented a force magnitude balance hypothesis for the M_A control of the coupling efficiency (see also Koskinen 2011). Variations in the plasma beta change the relative magnitude of the pressure force and the magnetic force in the magnetosheath that affects how flows are diverged. When the magnetic force dominates the plasma deviates increasingly and the fraction of the solar wind electric field that can impinge the magnetopause and the associated reconnection will decrease. This effect again decreases the coupling efficiency of low M_A ICMEs when compared to high M_A structures. However, Lavraud and Borovsky (2008) mentioned that increased magnetic tension forces in the magnetosheath accelerate plasma effectively around the magnetopause. The authors also pointed out that high velocity shear at the magnetopause creates favorable conditions for non-linear Kelvin-Helmholtz vortices (Lavraud and Borovsky 2008) that may increase the role of viscous interactions in transferring the energy (e.g., Hasegawa et al. 2004). As the flow speeds increase for low M_A conditions this effect could in turn enhance coupling efficiency for ICME-driven storms.

Rapid IMF fluctuations in sheaths, CIRS and HSSs can also enhance viscous interactions at the magnetopause as demonstrated e.g., by Borovsky and Funsten (2003) and Osmane et al. (2015) and lead to larger geoeffectivity. Turbulent conditions in the upstream solar wind could increase turbulence in the low-latitude boundary layer where the majority of the energy transfer occurs. This is also the region where field-aligned currents arise to the ionosphere and the vorticity increases the strength of these currents (e.g., Koskinen 2011). Large variations in IMF have also been suggested to trigger externally substorms (e.g., McPherron et al. 1986; Lyons et al. 1997), although more recent studies suggest that this association is rather a coincidence than causality (e.g., Morley and Freeman 2007; Newell and Liou 2011).

The role of solar wind dynamic pressure has also been highlighted in several studies. Increased solar wind dynamic pressure evidently compresses the whole magnetosphere (e.g., Shue et al. 1998), increasing magnetopause currents (e.g., Burton et al. 1975). Global MHD simulations by Palmroth et al. (2004) found evidence that increasing solar wind dynamic pressure increases the field aligned currents coupling the magnetosphere to ionosphere, and consequently the ionospheric Joule heating. Myllys et al. (2017) showed that solar wind dynamic pressure seems to inhibit polar cap potential from saturation during intense solar

wind driving electric fields. It also interesting to note that both simulations and observations suggest that coupling efficiency is higher when the solar wind speed makes the driving electric field or dynamic pressure large (Palmroth et al. 2010; Pulkkinen et al. 2015; Myllys et al. 2016). The above findings again give support that sheaths have stronger coupling efficiency than ICMEs.

4.3 Bow Shock Configuration and Structures

The bow shock configuration has also an important role in controlling the coupling efficiency. The way the plasma and magnetic field change at the bow depends strongly on whether the shock is quasi-perpendicular or quasi-parallel. This is defined by the upstream solar wind magnetic field. The transition through the bow shock and the magnetosheath has been studied in detail for MCs by Turc et al. (2015) who showed that their magnetic structure alters significantly behind quasi-parallel regime of the bow shock. This alteration can even reverse the sign of B_Z. However, the magnetic fields in MCs are oriented in a way that they tend to be associated with quasi-perpendicular sub-solar bow shock configurations (e.g., Turc et al. 2016). It is yet unclear how the bow shock responds to turbulent drivers (sheaths, CIRs and HSSs) as due to rapid IMF fluctuations the bow shock configuration is expected to vary over relatively short time scales. As discussed in the previous section the shock angle controls the physics of the shock, and hence, the magnetosheath has very different properties behind quasi-perpendicular and quasi-parallel sections of the bow shock (e.g., Walsh et al. 2012; Dimmock et al. 2015).

We also note that the vicinity of the bow shock and magnetosheath have complex internal structure. In particular the foreshock associated with the quasi-parallel bow shock and the magnetosheath behind are populated by various localized structures, such as cavitons, shocklets, Short Large Amplitude Magnetic Structures (SLAMS), hot flow anomalies, spontaneous hot flow anomalies and jets (e.g., Hietala et al. 2009; Blanco-Cano et al. 2011; Omidi et al. 2013; Zhang et al. 2013). It is expected that these structures affect how upstream solar wind plasma and magnetic field change before reaching the magnetopause. However, is not yet clear to what extent they can regulate coupling efficiency and how solar wind conditions and the type of the large-scale solar wind driver control their formation and evolution.

4.4 Plasma Sheet Density and Ring Current Composition

Additional factor that we have not discussed so far, but that may significantly affect the storm magnitude are the density in the Earth's inner plasma sheet and the composition of the ring current. The importance of both of these may vary depending on the large-scale solar wind structure driving the storm. Firstly, the plasma sheet density is known to correlate with the solar wind density, and in particular the sustained northward IMF periods are associated with a "super-dense" plasma sheet (Terasawa et al. 1997; Borovsky et al. 1997). The later convection of this high density plasma inwards toward the Earth may build up ring current and intensify the storm (e.g., Farrugia et al. 2006; Lavraud et al. 2006). The importance of plasma sheet density for contributing to the ring current has been also demonstrated in several simulation studies (e.g., Liemohn et al. 2001; Kozyra et al. 2002; Jordanova et al. 2009). We note that a sheath with primarily northward fields and high densities followed by an MC with southward fields can provide particularly favorable conditions for first creating a super-dense plasma sheet and subsequent sustained convection building a strong ring current. Another possible structure is helmet streamer related CIRs that are generally preceded by high densities (Sect. 3.2.3).

While the quiet time ring current is carried mainly by protons, the contribution from oxygen ions increases dramatically during magnetic storms and with increasing storm magnitude (Daglis et al. 1999). As shown in Kamide et al. (1998b) O^+ comprises only about 10% of the ring current energy density during quiet times, but during extreme storms the contribution can increase up to about 70%. The H^+ ions in the ring current originate both from the solar wind and from the ionosphere, while O^+ is primarily of ionospheric origin. As ICMEs generally drive stronger storms than CIRs, it would be expected that ICME related storms would have larger O^+ content than CIR storms. This was indeed demonstrated statistically by Denton et al. (2006) using LANL/MPA data. In addition, we suggest that high solar wind densities in sheaths could result in particularly oxygen-rich ring current as it was shown by Daglis and Kozyra (2002) that dynamic pressure pulses are related to the enhanced O^+ outflow from the ionosphere.

4.5 Energy Partitioning and the Large-Scale Driver Type

Different structures lead also to different storm energy partitioning: CIR- and HSS-driven storms dissipate more energy into the ionosphere through Joule heating and particle precipitation, while ICMEs dissipate more energy into the ring current (e.g., Turner et al. 2009; Guo et al. 2011; Hajra et al. 2014). These studies did not separate contributions from ICMEs and their sheaths. It is, however, expected that turbulent sheaths dissipate more energy to the ionosphere, similar to CIRs and HSSs. This was also suggested by Huttunen et al. (2002) and Huttunen and Koskinen (2004) who demonstrated that ICMEs cause relatively stronger response to the ring current index Dst, while sheaths produce a stronger response to high-latitude auroral indices and to Kp.

As suggested by Kamide et al. (1998a) the ring current intensifies primarily due to prolonged convection and associated plasma transport during the southward IMF, not due to successive substorm injections. In addition, Tsurutani et al. (2003) reported the lack of substorm expansion phases for steady southward IMF intervals that are typical conditions during MCs. As a consequence, MCs are likely drivers of steady magnetospheric convection events, discussed in Introduction. Simulation studies that do not take into account substorm injections typically underestimate the modeled Dst, and this underestimation is clearly larger (by 20–30%) for CIR-driven storms when compared to ICME-driven storms (e.g., Liemohn et al. 2010; Jordanova et al. 2009; Cramer et al. 2013). This implies that substorm injections may play on average larger role in building up the ring current for CIR than ICME related storms. Another possible causes are for example the significant contribution from other current systems than the ring current to Dst (e.g., tail current and auroral currents). Hajra et al. (2014) also compared energy partitioning for CIRs and HSSs that drove HILDCAAs (see Sect. 3.2). The authors found that in HSSs more energy went into Joule heating than during CIRs-storms (67% and 49%, respectively), while both had comparable share to the ring current.

5 Interacting Large-Scale Structures

In previous sections we have examined geo-effective properties of ICMEs, shocks/sheaths and CIRs separately. Individually these structures usually lead to a one-step geomagnetic storm sequence with or without a sudden commencement followed by a main phase and then a recovery phase. A combination of these structures, however, is often seen in the solar wind that can give rise to a multi-step, enhanced geomagnetic storm (e.g., Burlaga et al. 1987;

Gonzalez et al. 1999; Echer and Gonzalez 2004; Zhang et al. 2007). Zhang et al. (2007) divided their 77 ICME-related intense storms (Dst < -100 nT) to single and multiple types, depending on whether the storm was caused by a single ICME associated with a single CME at the Sun, or by multiple ICMEs and CMEs. While they found that the majority of intense ICME-driven storms were single type (69%), almost one-third of them are still caused by multiple ICMEs. We also note that Zhang et al. (2007) classification did separate ICMEs interacting with CIRs and HSSs.

The "perfect storm" scenario proposed by Liu et al. (2014a, 2015) refers to a combination of circumstances that can result in a particular aggravation of the situation. There are many combinations of circumstances that can occur to make an event more geo-effective, including pileup of events, preconditioning of the upstream solar wind for CME propagation, shock enhancement of pre-existing southward magnetic fields, and following high-speed streams causing compression. The "perfect storm" scenario can be frequent enough for us to worry about because complex structures with these combinations are common in the solar wind.

Burlaga et al. (2001, 2002) defined complex ejecta as fast, transient flows resulting from interactions between successive CMEs. Such interactions are a frequent phenomenon in interplanetary space especially near solar maximum (e.g., Liu et al. 2013). The readers are directed to Manchester et al. 2017, this issue (and references therein) for discussions of the physics about CME-CME interactions. Complex ejecta, in general, do not have well-ordered magnetic fields, but may have a sustained period of enhanced southward magnetic fields produced by CME-CME interactions (e.g., Farrugia and Berdichevsky 2004; Wang et al. 2003; Liu et al. 2014a; Lugaz and Farrugia 2014). As sustained southward magnetic field is a key factor in geomagnetic storm generation, complex ejecta can be very geo-effective given their prolonged duration. They have been considered as a trigger of two-step geomagnetic storms (e.g., Farrugia and Berdichevsky 2004; Farrugia et al. 2006; Liu et al. 2014b), in addition to the sheath-ejecta mechanism (Tsurutani et al. 1988). Complex ejecta are also often associated with a high solar wind densities and consequently high Alfvén Mach numbers, due to interactions between CMEs that are likely to enhance solar wind—magnetosphere coupling, see previous section.

An extreme example of complex ejecta formed by CME-CME interactions is the 2012 July 23 event (Liu et al. 2014a), see Fig. 12. The peak solar wind speed downstream of the shock measured in situ at STEREO A was about 2250 km s^{-1}, and the magnetic field inside the ejecta was as high as 109 nT (e.g., Russell et al. 2013; Baker et al. 2013; Liu et al. 2014a). Both the peak solar wind speed and the maximum magnetic field strength are among the largest ever measured near 1 AU. Liu et al. (2014a) suggest that the extremely enhanced ejecta magnetic field was caused by the in-transit interaction between two closely launched eruptions. They also indicate that the unusually high speed at STEREO A was due to preconditioning of the upstream solar wind by another earlier CME, which produced a low-density environment with radial magnetic fields for the propagation of the 2012 July 23 complex CME. Further analyses of the shock properties and propagation behavior give results consistent with this pre-conditioning idea (Temmer and Nitta 2015; Cash et al. 2015; Riley et al. 2016). If the event had hit the Earth, it would have generated a geomagnetic storm comparable to or even larger than the Carrington event (Baker et al. 2013; Liu et al. 2014a).

A shock overtaking a preceding ejecta can enhance the speed and the pre-existing southward magnetic field inside the ejecta, an idea for increased geo-effectiveness dating back several decades (Burlaga 1991; Lepping et al. 1997; Vandas et al. 1997). This could be a special case of complex ejecta (e.g., Liu et al. 2012, 2014b; Möstl et al. 2012; Harrison et al.

2012; Webb et al. 2013), but the shock may or may not be associated with a following CME. Shock compression of pre-existing southward magnetic fields can lead to a two-step geo-magnetic storm (e.g., Liu et al. 2014b). A statistical analysis indicates that 39% (19 out of 49 shocks) of shocks propagating inside ICMEs are associated with an intense geomagnetic storm (minimum $D_{st} < -100$ nT; Lugaz et al. 2015).

The geo-effectiveness of a CME can also be enhanced when the CME is compressed from behind by a CIR or a fast solar wind stream (e.g., Fenrich and Luhmann 1998; Webb et al. 2000; Kilpua et al. 2012; Liu et al. 2015; Kataoka et al. 2015). Similar to CME-CME interactions, this kind of compression can help in maintaining a strong ejecta magnetic field as well as a relatively high speed. As discussed in Sect. 3.2 whether this compression can enhance the storm magnitude depends on the ICME "flux rope type". Tail-part compression for NS-type MCs enhances southward magnetic fields, density and speed, and consequently solar wind dynamic pressure and M_A. All these can intensify the coupling efficiency and storm magnitude, see examples e.g., from Fenrich and Luhmann (1998) and Kilpua et al. (2012). In addition, the northward fields in the leading part of the cloud (and in the sheath) can contribute to the above-discussed preconditioning of the plasma sheet density and in-tensify the subsequent storm. Sheaths may also pre-condition the magnetosphere favorably for SN-type clouds. Storms driven by SN-type MCs with geoeffective sheaths often feature two-step Dst development (e.g., Kamide et al. 1998c), while for NS-type MCs two separate magnetic storms are expected as the magnetosphere has time to return to its quiet-time state during the northward fields in the leading part of the MC. Interactions between a CME and the following SIR or another CME can also deflect the CME in interplanetary space and affect its ability to drive magnetospheric storm.

However, it is not obvious how much preceding intensification of the ring current would contribute to the storm intensification. Kozyra et al. (2002) performed a kinetic ring current drift-loss simulation of a strong magnetic storm on 4–6 June 1991 whose main phase was created by three consecutive southward B_Z excursions. The authors found that the previous intensifications of the ring current were quickly swept by the enhanced magnetospheric con-vection associated with the next B_Z excursion. This is because during sustained southward IMF the ions in the inner magnetosphere that constitute the ring current are mainly on open drift paths and they are lost at the dayside magnetopause (e.g., Liemohn et al. 2001). Only the weakening or northward turning of the IMF will trap these particles on closed drift paths. However, Kozyra et al. (2002) study emphasised the importance of the plasma sheet density variations in subsequent intensifications in altering the ring current development. This can be an important factor in understanding and forecasting the magnetospheric response for interacting structures.

In turn, magnetic flux erosion by magnetic reconnection at the MC boundaries may re-duce significantly its expected geomagnetic response. Whether the reconnection can occur depends on the magnetic shear, i.e., the relative orientation of the magnetic field between the flux rope and the ambient solar wind. Figure 15 shows a parametric study by Lavraud et al. (2014) of the modeled Dst response for SN-type MCs having different levels of erosion. It is clear that the Dst response quickly weakens with the increasing erosion. The authors also noted that the erosion may be absent even when the magnetic shear would be favorable if the current sheet at the MC boundary is too thick. However, it seems that erosion is a relatively common process: The detailed statistical analysis of 50 MCs by Ruffenach et al. (2015) showed that nearly 30% of them showed reconnection signatures at their boundaries and the average erosion was significant, 40% of the total azimuthal flux.

The combinations can be more complex involving multiple solar wind structures. For example, the 2015 March 17 intense geomagnetic storm may have resulted from the inter-action between two successive CMEs (Liu et al. 2015) or with the interaction of a CME

Fig. 15 The panels show (**a**) solar wind driving electric field from the Lundquist flux rope model with maximum magnetic field of 23 nT and speed 400 km/s, (**b**) Dst response as modeled using the O'Brien and McPherron (2000) model, (**c**) the rate of change in Dst. The colors depict level of erosion. *Black* is the non-eroded case, while the *red* is the most eroded case. Figure is from Lavraud et al. (2014)
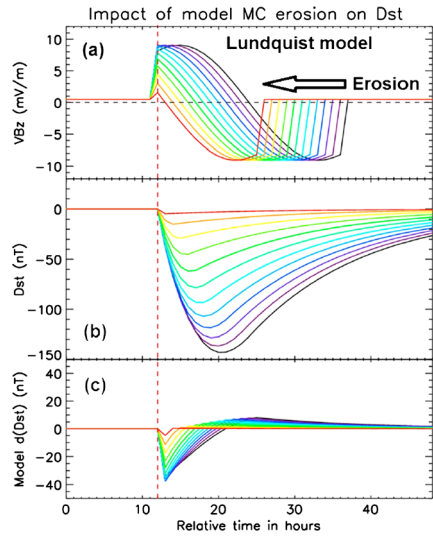
with the heliospheric plasma sheet (Kataoka et al. 2015) (or having the both aspects), plus the compression by a high-speed stream from behind. Wang et al. (2016) also point out that the CME associated with the main magnetic cloud deflected significantly toward the Earth, which contributed to the unexpected geoeffectiveness of this event. Another intense geomagnetic storm, which occurred on 2015 June 22, was caused by a combination of several preceding shocks with a following CME (Liu et al. 2015). These preceding shocks amplified the southward magnetic field, although fluctuating, as well as the solar wind density, which created favorable conditions for a major geomagnetic storm. A sheath-ejecta-ejecta and a sheath-sheath-ejecta combinations are proposed for the multi-step development of geomagnetic storms based on the studies of the 2015 March 17 and June 22 events (Liu et al. 2015). All these findings reinforce the idea and importance of the "perfect storm" scenario for severe space weather.

6 Solar Cycle and Seasonal Variations

To understand long-term variations in space weather it is important to understand how the frequencies and magnitudes of storms associated with different drivers vary with solar cycle. CIR- and ICME-driven storms exhibit clearly different solar cycle trends that are connected to their different origins, discussed in Sect. 2. Properties of interplanetary shocks and sheaths, and consequently their geomagnetic effects, vary also strongly with solar cycle.

6.1 Solar Cycle Variations

The number of recurrent, generally small to medium CIR/HSS-driven magnetic storms peaks in the declining phase of solar activity cycle (e.g., Tsurutani et al. 1995; Gonzalez et al. 1999; Borovsky and Denton 2006; Zhang et al. 2008; Richardson and Cane 2012). As CIRs arise when slow and fast streams interact, their solar cycle variations are connected to the variations in the occurrence and latitudinal distribution of coronal holes and the helmet streamer structure. As discussed earlier the coronal hole characteristics are controlled by
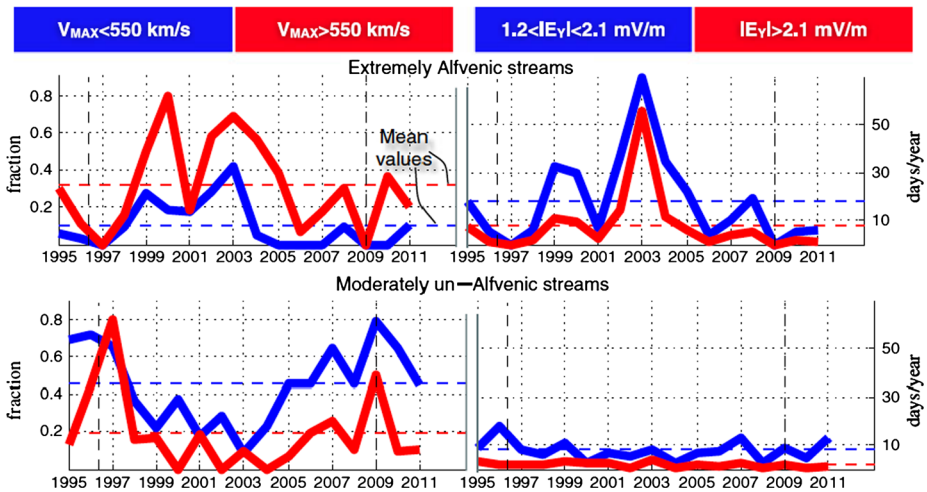
Fig. 16 Yearly distribution of solar wind speeds and electric field for (*Top*) extremely Alfvénic streams and (*Bottom*) moderately non-Alfvénic streams. Figure is from Snekvik et al. (2013)

the poloidal (meridional) component of the Sun's global magnetic field that maximises in the late declining phase and at solar minimum. CIRs do not show clear solar cycle trend in their properties, but they have a tendency towards lower speed gradients, magnetic fields, dynamic pressure and durations at solar minimum than at other times, in particular in the late declining phase (see Fig. 5 in Jian et al. 2006b). Hence, although CIRs are frequent also at solar minimum they drive fewer magnetic storms as they are weaker at this time.

As discussed in Sect. 3.2 the geoeffectivity of HSSs is largely controlled by Alfvénicity. Snekvik et al. (2013) showed that the Alfvénicity of HSSs varies substantially with solar cycle. Figure 16 shows that near solar maximum and early declining phase most fast streams are extremely Alfvénic, while in the late declining phase and at solar minimum fast streams are largely non-Alfvénic. At solar minimum also the number of slow-HSSs increases (i.e. streams that have considerable speed gradient to form CIRs, but whose peak speed is < 550 km/s). The figure also shows that Alfvénic streams produce most significant driving electric fields. As discussed in Snekvik et al. (2013) these variations are presumably related to the variations in the sources of the fast wind, i.e., whether they originate from mid/low-latitude coronal holes or from equatorward extensions of polar coronal holes.

In turn, ICME-related storms follow more closely the sunspot number (SSN). This overall correlation is expected as the occurrence of the fast and strong CMEs from solar active regions follows the evolution of the toroidal component of the Sun's global magnetic field (e.g., Gopalswamy et al. 2004; Webb and Howard 2012). CMEs originate also outside active regions, from helmet streamers and in association with quiet Sun filament disappearances (e.g., Subramanian and Dere 2001; Webb and Howard 2012; Liu et al. 2016) and hence, CMEs are observed in all phases of the solar activity cycle. Solar cycle trends in the ICME occurrence rate and properties naturally reflects those for CMEs (e.g., Webb and Howard 2012), and as a consequence, ICMEs are generally faster and stronger, and more frequent near solar maximum than near solar minimum (e.g., Cane and Richardson 2003; Liu et al. 2005; Jian et al. 2006b). However, the variations in the near ecliptic ICME rate diverge occasionally from the variations in the CME rate. For example, surprisingly many ICMEs were observed near the ecliptic during solar minimum (Kilpua et al. 2011). This is because at

this time the helmet streamer belt was confined close to the equator and large polar coronal holes effectively deflected high-latitude CMEs towards lower latitudes (see Manchester et al. 2017, this issue). At solar maximum times the deflection is more random and CME sources are distributed more evenly at all latitudes (e.g., von Steiger et al. 2005; Webb and Howard 2012). Gonzalez et al. (2011) separated also the effect from MCs and sheaths when they studied the importance of different large-scale solar wind structures as drivers of intense magnetic storms (Dst < −100 nT) during Solar Cycle 23. They found that in the rising phase MCs and ICME sheaths were the most important storm drivers, near solar maximum sheaths drove most storms, and in the declining phase MCs and CIRs caused the majority of the intense activity.

However, the exact correlation between the ICME-related storms and the SSN is more complex; rather than peaking exactly at the SSN maximum intense storms have a double-peaked occurrence distribution, with the largest number of storms occurring a few years before and after the SSN peak (e.g., Newton and Milsom 1954; Le et al. 2013). In the Le et al. (2013) study the majority of storms in all investigated magnitude categories occurred in the declining solar activity phase. Kilpua et al. (2015b) and Gonzalez et al. (1990) also found that intense storms occur most frequently in the declining phase, but in these studies the most extreme storms occurred at or relatively close to solar maximum. In addition, the authors did not report that drastic difference between the descending and ascending phases as in Le et al. (2013). These partly contradicting results might stem from how solar maximum is defined, and the fact that many solar cycles feature multi-peaked SSN maxima. In particular, the likelihood for interactions between multiple CMEs increases clearly near solar maximum. As discussed in Sect. 5 such interactions combined to "preconditioning" of the heliosphere by previous CMEs is a particularly likely scenario to lead to the most extreme space weather events ("perfect storm scenario" by Liu et al. (2014a)). The bias towards the declining phase for intense (Dst < −100 nT) storms may also result from the CIRs and fast streams enhancing the geomagnetic response of the preceding ICME. We also note that double-peaked solar cycles have been explained to result from the asymmetric evolution between the northern and southern solar hemispheres. Gopalswamy et al. (2015), however, highlighted that there is necessarily no direct link to variations in the CME rates and properties. The authors studied the properties of CMEs and ICME-driven storms during the multi-peaked Solar Cycle 24 and they found that more geomagnetic storms and more energetic CMEs occurred during the first weaker SSN peak (2012) than during the subsequent stronger peak (2014).

The dependence between the yearly mean SSN and the yearly number of Storm Sudden Commencements (SSCs) for a large data set between 1858 and 2014 is shown in Fig. 17. The figure reveals a clear positive correlation, which presumably arises from the fact that a large fraction SSCs are related to fast forward shocks (see Introduction) whose variations follow closely those in SSN. The clear correlation between the yearly number of fast forward shocks detected in the near-Earth solar wind with the SSN is illustrated in the bottom panel of Fig. 18 that is based on Kilpua et al. (2015a). The comparison of the top panels shows that the ICME-associated forward shocks dominate the distribution and are the cause of the solar cycle dependence. In turn, reverse shocks are almost exclusively associated with CIRs. While there is a clear correlation between SSCs and SSN, as discussed in Introduction, SSCs are seen to occur also without interplanetary shocks, evidently driven by solar wind dynamic pressure pulses at the leading edges of ICMEs and CIRs without an accompanying shock wave. As shown by Zuo et al. (2015) the variations in the number of solar wind dynamic pressure pulses are also roughly in phase with solar cycle, consistent with the results in Fig. 17.

Fig. 17 The correlation between the yearly sunspot number and Storm Sudden Commencements (SSCs) between 1858 and 2014. The red line represents the best linear fit to the data. (Sunspot numbers from: http://www.sidc.be/silso/datafilesand SSCs from ftp://ftp.ngdc.noaa.gov/STP/SOLAR_DATA/SUDDEN_COMMENCEMENTS/SCYEAR

$$N_{SSC} = 11.68 + 0.169 \times R$$
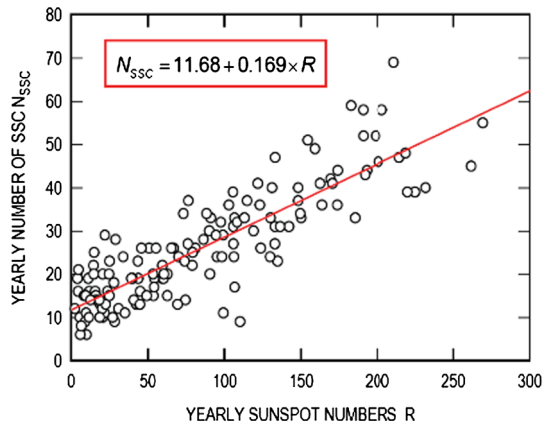
Fig. 18 Annual number of (**a**) CME-associated shocks, (**b**) CIR associated shocks, and (**c**) the total number of shocks. Red histograms show the fast forward shocks and *blue panels* fast reverse shocks. Note the very different scales between panels (**a**) and (**c**) on one hand and panel (**b**) on the other. Figure based on data in Kilpua et al. (2015a)
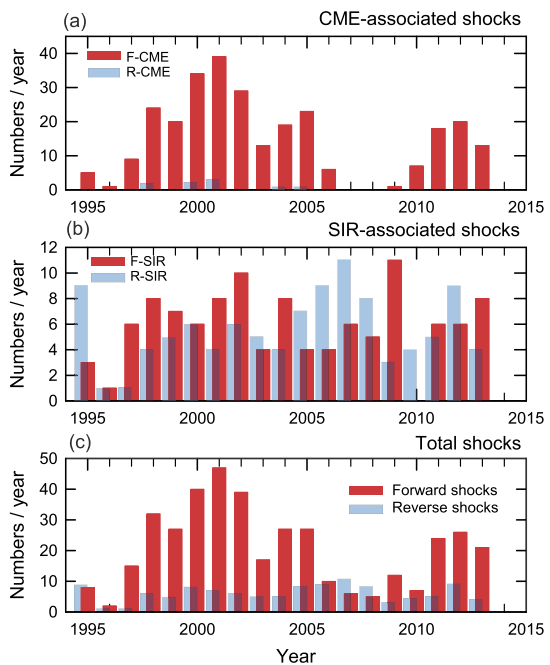
In Sect. 3.2 we highlighted that the flux rope type of the MC is highly important for its space weather response. The occurrence of bipolar MCs has a clear trend with the 22-year solar magnetic cycle (e.g., Bothmer and Schwenn 1998; Huttunen et al. 2005; Li et al. 2011). The SN-type (NS-type) MCs dominate from the late declining phase of even (odd) numbered solar cycles to the next rising phase. At solar maximum a mixture of SN- and NS-type clouds are observed because the Sun's global magnetic field changes the sign. For unipolar clouds no similar solar cycle trend has been reported. However, Kilpua et al. (2012) noted that during the minimum and early rising phases of Solar Cycle 24 a large fraction of unipolar MCs had their fields northward when compared to previous similar solar cycle phases, which may have contributed to low geomagnetic activity during the early rising phase of cycle 24. On average, the SN and NS type clouds have similar magnitude in their geospace

responses, but as discussed in Sect. 3.2 their geoefficiency is controlled in a different way with the kinematic evolution of the CME and the ambient solar wind structure. One additional, interesting solar cycle trend related to MCs, is their fraction from all ICMEs; near solar minimum roughly all ICME are MCs, while at solar maximum the fraction of MCs decreases dramatically to about 10–20% (e.g., Cane and Richardson 2003; Huttunen et al. 2005; Jian et al. 2006a).

6.2 Seasonal Variations

Geomagnetic activity has also seasonal variations that are commonly connected to the changes in the relative orientation between the Sun and the Earth, often called as Russell and McPherron effect (Russell and McPherron 1973). CIR-driven storms have a clear seasonal effect and the majority of CIR-storms occur during "favoured" IMF directions, i.e., close to fall and spring equinoxes (e.g., Alves et al. 2006; Richardson et al. 2006; Zhang et al. 2008). For example, Alves et al. (2006) reported that roughly 50% of CIRs are followed by at least a moderate storms (Dst < -50 nT) during equinoxes, compared to before mentioned roughly 30% geoeffectiveness of CIRs when all time periods are considered. According to Richardson et al. (2006) the majority of cases when CIRs cause intense (Dst < -100 nT) storms occur during equinoxes. In turn, large ICME-driven storms are usually caused by strongly out-of-ecliptic IMF that has southward component over pro-longed periods, and as a consequence, for ICME driven storms the dipole tilt effect has only a minor contribution (Lockwood et al. 2015). A partly contrary view to seasonal variations has been suggested by Crooker (2000). The authors argue that about two-thirds of the semi-annual variations are attributed to the decreasing coupling efficiency at the solstices, rather than creation of stronger southward IMF at the equinoxes.

6.3 Variations with the Strength of the Solar Cycle

Kilpua et al. (2015b) also examined the relationship of strong magnetic storms with the strength of the solar cycle (as measured by the sunspot number). They found that there is a positive correlation between the strength of solar cycles and magnetic storms. The correlation however decreases with increasing storm magnitude and becomes negligible for the most extreme storms. Hence, there can be some extreme storms even during weak solar cycles (e.g., Carrington storm in 1859, see Sect. 2), but in these cases also the large storms avoid the solar cycle minimum. To investigate long-term driving trends of geomagnetic activity by different large-scale solar wind structures, one viable option is to use the principal component and the independent component analysis of local geomagnetic indices (Holappa et al. 2014)

7 Discussion and Future Outlook

In this article we have reviewed geoeffective properties of large-scale interplanetary structures; Interplanetary coronal mass ejections (ICMEs), shocks/sheaths, Corotating Interaction Regions (CIRs), and High-Speed Streams (HSS) and their combinations. We have demonstrated that these structures are in many respects very different considering their origin, solar wind properties, solar wind—magnetosphere coupling efficiency, geospace responses and solar cycle trends. We discuss below some of the key points highlighted in this review, in particular in the context of understanding and predicting space weather.

We highlight that sheaths and ICMEs, in particular their subset magnetic clouds (MCs), represent very distinct modes of solar wind forcing of the magnetosphere, and therefore, it is of paramount importance to separate these structures. Sheaths are characterized by turbulent magnetic fields and large Alfvén Mach (M_A) numbers and dynamic pressure, while MCs exhibit distinctly smoother driving and generally low dynamic pressure and low M_A conditions.

Based on the existing literature is seems that the "sheath-like" solar wind conditions are associated to more efficient solar wind—magnetosphere coupling. However, due to combination of strong fields and high speeds, and potential to provide sustained southward magnetic fields, MCs are key drivers of intense magnetic storms, in particular when the storm level is determined by Dst. In turn, sheaths deposit most energy in the high-latitude ionosphere. CIRs have more sheath-like conditions, but due to weaker fields and more rapidly fluctuating fields they drive mostly weak to moderate activity, while ICME sheaths cause frequently intense storms. As the large-scale structures often arrive in sequences (e.g., a shock, sheath, MC followed by a CIR and a high-speed stream), the Earth's magnetosphere can encounter rapidly changing forcing conditions and responses.

Two basic steps can be identified when predicting the space weather response of large-scale interplanetary structures: (1) Long-lead time (1–3 days) prediction of their solar wind conditions in the near-Earth solar wind upstream of the bow shock, and (2) Prediction of the details of geomagnetic activity using the near-Earth solar wind observations that are typically available from the Lagrangian point L1 (e.g., Wind, ACE, DSCOVR), i.e., providing lead-times of approximately of 30 min–1 hour.

Some aspects pertaining to Step (1) have improved significantly lately, e.g., numerical heliospheric simulations using information based on the multi-spacecraft CME modeling provide now more accurate CME impact time and details as well as estimates on the overall magnetic field magnitude and plasma parameters. However, the status of long lead-time predictions is currently very limited and in particular the key parameter, the magnetic field north-south component, cannot be measured in the corona, nor predicted in any practical way for space weather purposes. In addition, as discussed in this paper, recent studies also emphasize that to estimate the geospace response it is pivotal to have a detailed knowledge of several other solar wind parameters, including fluctuation levels. Predicting these well in advance would likely require going beyond the MHD-based simulations as kinetic processes can play a significant role in producing variations in particular in turbulent sheath-like drivers and also in regulating the global structure of drivers. Or at least, a very high-resolution grids in MHD simulations are needed.

While the basic processes how the solar wind couples to the magnetosphere are now relatively well understood, recent studies underline the complexity of this coupling. One big issue is the transition through the bow shock and the subsequent propagation through the magnetosheath. As discussed here, the bow shock configuration and the upstream solar wind conditions play a major role in controlling how plasma and magnetic field change. While ICMEs tend to produce quasi-perpendicular bow shock that largely preserves their magnetic field characteristics, it is currently an open issue how the bow shock responds to fluctuating drivers (sheaths, CIRs, and HSSs). Another significant open question is how solar wind conditions control the magnetosheath conditions and conditions in the low-latitude boundary layer through which the majority of the energy transfer occurs and where field-aligned currents arise to the ionosphere. In the future we need more physics-based understanding of details of these coupling processes as a function of upstream solar wind driving conditions and understanding how local and kinetic scale processes and structures regulate global magnetosheath conditions and reconnection details at the magnetopause.

Interactions between the structures introduces a further challenge, and the details of resulting complex structures are largely beyond the current modeling capabilities. As discussed here, there are several processes how interaction between the structures can lead to enhancements of geoeffective properties and solar wind—magnetosphere coupling efficiency and aggravation of the resulting magnetic storm.

Many of the issues discussed above and in particular those involved in interacting structures pertain to "grand challenges in space physics" discussed e.g., by von Steiger (2013), including complexity of space weather, magnetic reconnection, boundaries and collisionless shocks. In particular, this paper emphasizes that although significant progress has been made in many of the above discussed problems, individually, one of the greatest challenges is to unify different aspects into an overall picture.

References

B.-H. Ahn, S.-I. Akasofu, Y. Kamide, The Joule heat production rate and the particle energy injection rate as a function of the geomagnetic indices AE and AL. J. Geophys. Res. **88**, 6275–6287 (1983). doi:10.1029/JA088iA08p06275

S.-I. Akasofu, Interplanetary energy flux associated with magnetospheric substorms. Planet. Space Sci. **27**, 425–431 (1979). doi:10.1016/0032-0633(79)90119-3

S.-I. Akasofu, Energy coupling between the solar wind and the magnetosphere. Space Sci. Rev. **28**, 121–190 (1981). doi:10.1007/BF00218810

C.W. Allen, Relation between magnetic storms and solar activity. Mon. Not. R. Astron. Soc. **104**, 13 (1944). doi:10.1093/mnras/104.1.13

M.V. Alves, E. Echer, W.D. Gonzalez, Geoeffectiveness of corotating interaction regions as measured by Dst index. J. Geophys. Res. Space Phys. **111**, A07S05 (2006). doi:10.1029/2005JA011379

A. Badruddin, Z. Falak, Study of the geoeffectiveness of coronal mass ejections, corotating interaction regions and their associated structures observed during Solar Cycle 23. Astrophys. Space Sci. **361**, 253 (2016). doi:10.1007/s10509-016-2839-4

D.N. Baker, A.J. Klimas, D.A. Roberts, Examination of time-variable input effects in a nonlinear analogue magnetosphere model. Geophys. Res. Lett. **18**, 1631–1634 (1991). doi:10.1029/91GL01048

D.N. Baker, X. Li, A. Pulkkinen, C.M. Ngwira, M.L. Mays, A.B. Galvin, K.D.C. Simunac, A major solar eruptive event in July 2012: defining extreme space weather scenarios. Space Weather **11**, 585–591 (2013). doi:10.1002/swe.20097

S.D. Bale, M.A. Balikhin, T.S. Horbury, V.V. Krasnoselskikh, H. Kucharek, E. Möbius, S.N. Walker, A. Balogh, D. Burgess, B. Lembège, E.A. Lucek, M. Scholer, S.J. Schwartz, M.F. Thomsen, Quasi-perpendicular shock structure and processes. Space Sci. Rev. **118**, 161–203 (2005). doi:10.1007/s11214-005-3827-0

A. Balogh, P. Riley, *Overview of Heliospheric Shocks, in Cosmic Winds and the Heliosphere* (University of Arizona Press, Tucson, 1997)

A. Balogh, E.J. Smith, B.T. Tsurutani, D.J. Southwood, R.J. Forsyth, T.S. Horbury, The heliospheric magnetic field over the South polar region of the Sun. Science **268**, 1007–1010 (1995). doi:10.1126/science.268.5213.1007

A. Balogh, V. Bothmer, N.U. Crooker, R.J. Forsyth, G. Gloeckler, A. Hewish, M. Hilchenbach, R. Kallenbach, B. Klecker, J.A. Linker, E. Lucek, G. Mann, E. Marsch, A. Posner, I.G. Richardson, J.M. Schmidt, M. Scholer, Y.-M. Wang, R.F. Wimmer-Schweingruber, M.R. Aellig, P. Bochsler, S. Hefti, Z. Mikić, The solar origin of corotating interaction regions and their formation in the inner heliosphere. Space Sci. Rev. **89**, 141–178 (1999). doi:10.1023/A:1005245306874

J. Bartels, Terrestrial-magnetic activity and its relations to solar phenomena. Terr. Magn. Atmos. Electr. (J. Geophys. Res.) **37**, 1 (1932). doi:10.1029/TE037i001p00001

J.W. Belcher, L. Davis Jr., Large-amplitude Alfvén waves in the interplanetary medium, 2. J. Geophys. Res. **76**, 3534 (1971). doi:10.1029/JA076i016p03534

X. Blanco-Cano, P. Kajdič, N. Omidi, C.T. Russell, Foreshock cavitons for different interplanetary magnetic field geometries: simulations and observations. J. Geophys. Res. Space Phys. **116**, 09101 (2011). doi:10.1029/2010JA016413

X. Blanco-Cano, P. Kajdič, E. Aguilar-Rodríguez, C.T. Russell, L.K. Jian, J.G. Luhmann, Interplanetary shocks and foreshocks observed by STEREO during 2007–2010. J. Geophys. Res. Space Phys. **121**, 992–1008 (2016). doi:10.1002/2015JA021645

J.E. Borovsky, The rudiments of a theory of solar wind/magnetosphere coupling derived from first principles. J. Geophys. Res. Space Phys. **113**, 08228 (2008). doi:10.1029/2007JA012646

J.E. Borovsky, J. Birn, The solar wind electric field does not control the dayside reconnection rate. J. Geophys. Res. Space Phys. **119**, 751–760 (2014). doi:10.1002/2013JA019193

J.E. Borovsky, M.H. Denton, Differences between CME-driven storms and CIR-driven storms. J. Geophys. Res. Space Phys. **111**, A07S08 (2006). doi:10.1029/2005JA011447

J.E. Borovsky, M.H. Denton, The differences between storms driven by helmet streamer CIRs and storms driven by pseudostreamer CIRs. J. Geophys. Res. Space Phys. **118**, 5506–5521 (2013). doi:10.1002/jgra.50524

J.E. Borovsky, H.O. Funsten, Role of solar wind turbulence in the coupling of the solar wind to the Earth's magnetosphere. J. Geophys. Res. Space Phys. **108**, 1246 (2003). doi:10.1029/2002JA009601

J.E. Borovsky, K. Yakymenko, Substorm occurrence rates, substorm recurrence times, and solar wind structure. J. Geophys. Res. Space Phys. **122**, 2973–2998 (2017). doi:10.1002/2016JA023625

J.E. Borovsky, R.J. Nemzek, R.D. Belian, The occurrence rate of magnetospheric-substorm onsets—random and periodic substorms. J. Geophys. Res. **98**, 3807–3813 (1993). doi:10.1029/92JA02556

J.E. Borovsky, M.F. Thomsen, D.J. McComas, The superdense plasma sheet: plasmaspheric origin, solar wind origin, or ionospheric origin? J. Geophys. Res. **102**, 22089–22106 (1997). doi:10.1029/96JA02469

V. Bothmer, R. Schwenn, The structure and origin of magnetic clouds in the solar wind. Ann. Geophys. **16**, 1–24 (1998). doi:10.1007/s00585-997-0001-x

O.J. Brambles, W. Lotko, B. Zhang, J. Ouellette, J. Lyon, M. Wiltberger, The effects of ionospheric outflow on ICME and SIR driven sawtooth events. J. Geophys. Res. Space Phys. **118**, 6026–6041 (2013). doi:10.1002/jgra.50522

D. Burgess, E.A. Lucek, M. Scholer, S.D. Bale, M.A. Balikhin, A. Balogh, T.S. Horbury, V.V. Krasnoselskikh, H. Kucharek, B. Lembège, E. Möbius, S.J. Schwartz, M.F. Thomsen, S.N. Walker, Quasi-parallel shock structure and processes. Space Sci. Rev. **118**, 205–222 (2005). doi:10.1007/s11214-005-3832-3

L.F.E. Burlaga, in *Magnetic Clouds*, ed. by R. Schwenn, E. Marsch (1991), p. 152

L. Burlaga, E. Sittler, F. Mariani, R. Schwenn, Magnetic loop behind an interplanetary shock—Voyager, Helios, and IMP 8 observations. J. Geophys. Res. **86**, 6673–6684 (1981). doi:10.1029/JA086iA08p06673

L.F. Burlaga, L. Klein, N.R. Sheeley Jr., D.J. Michels, R.A. Howard, M.J. Koomen, R. Schwenn, H. Rosenbauer, A magnetic cloud and a coronal mass ejection. Geophys. Res. Lett. **9**, 1317–1320 (1982). doi:10.1029/GL009i012p01317

L.F. Burlaga, K.W. Behannon, L.W. Klein, Compound streams, magnetic clouds, and major geomagnetic storms. J. Geophys. Res. **92**, 5725–5734 (1987). doi:10.1029/JA092iA06p05725

L.F. Burlaga, R.M. Skoug, C.W. Smith, D.F. Webb, T.H. Zurbuchen, A. Reinard, Fast ejecta during the ascending phase of solar cycle 23: ACE observations, 1998–1999. J. Geophys. Res. **106**, 20957–20978 (2001). doi:10.1029/2000JA000214

L.F. Burlaga, S.P. Plunkett, O.C. St. Cyr, Successive CMEs and complex ejecta. J. Geophys. Res. Space Phys. **107**, 1266 (2002). doi:10.1029/2001JA000255

R.K. Burton, R.L. McPherron, C.T. Russell, An empirical relationship between interplanetary conditions and Dst. J. Geophys. Res. **80**, 4204–4214 (1975). doi:10.1029/JA080i031p04204

H.V. Cane, I.G. Richardson, Interplanetary coronal mass ejections in the near-Earth solar wind during 1996-2002. J. Geophys. Res. Space Phys. **108**, 1156 (2003). doi:10.1029/2002JA009817

H.V. Cane, I.G. Richardson, G. Wibberenz, Helios 1 and 2 observations of particle decreases, ejecta, and magnetic clouds. J. Geophys. Res. Space Phys. **102**, 7075–7086 (1997). doi:10.1029/97JA00149

R.C. Carrington, Description of a singular appearance seen in the Sun on September 1, 1859. Mon. Not. R. Astron. Soc. **20**, 13–15 (1859). doi:10.1093/mnras/20.1.13

M.D. Cash, D.A. Biesecker, V. Pizzo, C.A. Koning, G. Millward, C.N. Arge, C.J. Henney, D. Odstrcil, Ensemble modeling of the 23 July 2012 coronal mass ejection. Space Weather **13**, 611–625 (2015). doi:10.1002/2015SW001232

J.K. Chao, R.P. Lepping, A correlative study of ssc's, interplanetary shocks, and solar activity. J. Geophys. Res. **79**, 1799 (1974). doi:10.1029/JA079i013p01799

S. Chapman, V.C.A. Ferraro, The electrical state of solar streams of corpuscles. Mon. Not. R. Astron. Soc. **89**, 470 (1929). doi:10.1093/mnras/89.5.470

E.W. Cliver, L. Svalgaard, The 1859 solar-terrestrial disturbance and the current limits of extreme space weather activity. Sol. Phys. **224**, 407–422 (2004). doi:10.1007/s11207-005-4980-z

G.T. Cocconi, K. Greisen, S. Hayakawa, P. Morrison, The cosmic ray flare effect. Nuovo Cimento **8**, 161–168 (1958)

W.D. Cramer, N.E. Turner, M.-C. Fok, N.Y. Buzulukova, Effects of different geomagnetic storm drivers on the ring current: CRCM results. J. Geophys. Res. Space Phys. **118**, 1062–1073 (2013). doi:10.1002/jgra.50138

S.R. Cranmer, Coronal holes and the high-speed solar wind. Space Sci. Rev. **101**, 229–294 (2002)

N.U. Crooker, Solar and heliospheric geoeffective disturbances. J. Atmos. Sol.-Terr. Phys. **62**, 1071–1085 (2000). doi:10.1016/S1364-6826(00)00098-5

N.U. Crooker, C.-L. Huang, S.M. Lamassa, D.E. Larson, S.W. Kahler, H.E. Spence, Heliospheric plasma sheets. J. Geophys. Res. Space Phys. **109**, 03107 (2004). doi:10.1029/2003JA010170

N.U. Crooker, S.K. Antiochos, X. Zhao, M. Neugebauer, Global network of slow solar wind. J. Geophys. Res. Space Phys. **117**, 04104 (2012). doi:10.1029/2011JA017236

J.J. Curto, T. Araki, L.F. Alberca, Evolution of the concept of sudden storm commencements and their operative identification. Earth Planets Space **59**, i–xii (2007)

I.A. Daglis, J.U. Kozyra, Outstanding issues of ring current dynamics. J. Atmos. Sol.-Terr. Phys. **64**, 253–264 (2002). doi:10.1016/S1364-6826(01)00087-6

I.A. Daglis, R.M. Thorne, W. Baumjohann, S. Orsini, The terrestrial ring current: origin, formation, and decay. Rev. Geophys. **37**, 407–438 (1999). doi:10.1029/1999RG900009

M.H. Denton, J.E. Borovsky, R.M. Skoug, M.F. Thomsen, B. Lavraud, M.G. Henderson, R.L. McPherron, J.C. Zhang, M.W. Liemohn, Geomagnetic storms driven by ICME- and CIR-dominated solar wind. J. Geophys. Res. Space Phys. **111**, A07S07 (2006). doi:10.1029/2005JA011436

A.P. Dimmock, K. Nykyri, H. Karimabadi, A. Osmane, T.I. Pulkkinen, A statistical study into the spatial distribution and dawn-dusk asymmetry of dayside magnetosheath ion temperatures as a function of upstream solar wind conditions. J. Geophys. Res. Space Phys. **120**, 2767–2782 (2015). doi:10.1002/2014JA020734

J.W. Dungey, Interplanetary magnetic field and the auroral zones. Phys. Rev. Lett. **6**, 47–48 (1961). doi:10.1103/PhysRevLett.6.47

E. Echer, W.D. Gonzalez, Geoeffectiveness of interplanetary shocks, magnetic clouds, sector boundary crossings and their combined occurrence. Geophys. Res. Lett. **31**, 09808 (2004). doi:10.1029/2003GL019199

E. Echer, W.D. Gonzalez, B.T. Tsurutani, Interplanetary conditions leading to superintense geomagnetic storms (Dst ≤ −250 nT) during Solar Cycle 23. Geophys. Res. Lett. **35**, L06S03 (2008a). doi:10.1029/2007GL0317

E. Echer, W.D. Gonzalez, B.T. Tsurutani, A.L.C. Gonzalez, Interplanetary conditions causing intense geomagnetic storms (Dst ≤ −100 nT) during Solar Cycle 23 (1996–2006). J. Geophys. Res. **113**, A05221 (2008b). doi:10.1029/2007JA012744

W. Ellis, On the relation between the diurnal range of magnetic declination and horizontal force and the period of solar spot frequency. Proc. R. Soc. Lond. Ser. I **63**, 64–78 (1898)

C. Farrugia, D. Berdichevsky, Evolutionary signatures in complex ejecta and their driven shocks. Ann. Geophys. **22**, 3679–3698 (2004). doi:10.5194/angeo-22-3679-2004

C.J. Farrugia, M.P. Freeman, L.F. Burlaga, R.P. Lepping, K. Takahashi, The Earth's magnetosphere under continued forcing—substorm activity during the passage of an interplanetary magnetic cloud. J. Geophys. Res. **98**, 7657–7671 (1993). doi:10.1029/92JA02351

C.J. Farrugia, V.K. Jordanova, M.F. Thomsen, G. Lu, S.W.H. Cowley, K.W. Ogilvie, A two-ejecta event associated with a two-step geomagnetic storm. J. Geophys. Res. Space Phys. **111**, 11104 (2006). doi:10.1029/2006JA011893

F.R. Fenrich, J.G. Luhmann, Geomagnetic response to magnetic clouds of different polarity. Geophys. Res. Lett. **25**, 2999–3002 (1998). doi:10.1029/98GL51180

S.E. Forbush, On the effects in cosmic-ray intensity observed during the recent magnetic storm. Phys. Rev. **51**, 1108–1109 (1937). doi:10.1103/PhysRev.51.1108.3

J. Geiss, G. Gloeckler, R. von Steiger, Origin of the solar wind from composition data. Space Sci. Rev. **72**, 49–60 (1995). doi:10.1007/BF00768753

T. Gold, Discussion on shock waves and rarefied gas dynamics, in *Gas Dynamics of Cosmic Clouds*. IAU Symposium, vol. 2 (1955), pp. 97–105

T. Gold, Magnetic storms. Space Sci. Rev. **1**, 100–114 (1962). doi:10.1007/BF00174637

H. Goldstein, On the field configuration in magnetic clouds, in *NASA Conference Publication*. NASA Conference Publication, vol. 228 (1983)

W.D. Gonzalez, B.T. Tsurutani, Criteria of interplanetary parameters causing intense magnetic storms (Dst of less than −100 nT). Planet. Space Sci. **35**, 1101–1109 (1987). doi:10.1016/0032-0633(87)90015-8

W.D. Gonzalez, A.L.C. Gonzalez, B.T. Tsurutani, Dual-peak solar cycle distribution of intense geomagnetic storms. Planet. Space Sci. **38**, 181–187 (1990). doi:10.1016/0032-0633(90)90082-2

W.D. Gonzalez, J.A. Joselyn, Y. Kamide, H.W. Kroehl, G. Rostoker, B.T. Tsurutani, V.M. Vasyliunas, What is a geomagnetic storm? J. Geophys. Res. **99**, 5771–5792 (1994). doi:10.1029/93JA02867

W.D. Gonzalez, A.L.C. de Gonzalez, A. Dal Lago, B.T. Tsurutani, J.K. Arballo, G.K. Lakhina, B. Buti, C.M. Ho, S.-T. Wu, Magnetic cloud field intensities and solar wind velocities. Geophys. Res. Lett. **25**, 963–966 (1998)

W.D. Gonzalez, B.T. Tsurutani, A.L. Clúa de Gonzalez, Interplanetary origin of geomagnetic storms. Space Sci. Rev. **88**, 529–562 (1999). doi:10.1023/A:1005160129098

W.D. Gonzalez, E. Echer, B.T. Tsurutani, A.L. Clúa de Gonzalez, A. Dal Lago, Interplanetary origin of intense, superintense and extreme geomagnetic storms. Space Sci. Rev. **158**, 69–89 (2011). doi:10.1007/s11214-010-9715-2

J.A. González-Esparza, A. Balogh, R.J. Forsyth, M. Neugebauer, E.J. Smith, J.L. Phillips, Interplanetary shock waves and large-scale structures: Ulysses' observations in and out of the ecliptic plane. J. Geophys. Res. **101**, 17057–17072 (1996). doi:10.1029/96JA00685

N. Gopalswamy, S. Nunes, S. Yashiro, R.A. Howard, Variability of solar eruptions during cycle 23. Adv. Space Res. **34**, 391–396 (2004). doi:10.1016/j.asr.2003.10.054

N. Gopalswamy, P. Makela, S. Akiyama, S. Yashiro, N. Thakur, CMEs during the two activity peaks in cycle 24 and their space weather consequences. Sun Geosph. **10**, 111–118 (2015)

J.T. Gosling, The solar flare myth. J. Geophys. Res. **98**, 18937–18950 (1993). doi:10.1029/93JA01896

J.T. Gosling, D.J. McComas, Field line draping about fast coronal mass ejecta—a source of strong out-of-the-ecliptic interplanetary magnetic fields. Geophys. Res. Lett. **14**, 355–358 (1987). doi:10.1029/GL014i004p00355

J.T. Gosling, V.J. Pizzo, Formation and evolution of corotating interaction regions and their three dimensional structure. Space Sci. Rev. **89**, 21–52 (1999). doi:10.1023/A:1005291711900

J.T. Gosling, V. Pizzo, S.J. Bame, Anomalously low proton temperatures in the solar wind following interplanetary shock waves—evidence for magnetic bottles? J. Geophys. Res. **78**, 2001 (1973). doi:10.1029/JA078i013p02001

J.T. Gosling, E. Hildner, R.M. MacQueen, R.H. Munro, A.I. Poland, C.L. Ross, Direct observations of a flare related coronal and solar wind disturbance. Sol. Phys. **40**, 439–448 (1975). doi:10.1007/BF00162390

J.T. Gosling, J.R. Asbridge, S.J. Bame, W.C. Feldman, Solar wind stream interfaces. J. Geophys. Res. **83**, 1401–1412 (1978). doi:10.1029/JA083iA04p01401

J.T. Gosling, D.J. McComas, J.L. Phillips, S.J. Bame, Geomagnetic activity associated with Earth passage of interplanetary shock disturbances and coronal mass ejections. J. Geophys. Res. **96**, 7831–7839 (1991). doi:10.1029/91JA00316

W.M.H. Greaves, H.W. Newton, On the recurrence of magnetic storms. Mon. Not. R. Astron. Soc. **89**, 641–646 (1929). doi:10.1093/mnras/89.7.641

J. Guo, X. Feng, J. Zhang, P. Zuo, C. Xiang, Statistical properties and geoefficiency of interplanetary coronal mass ejections and their sheaths during intense geomagnetic storms. J. Geophys. Res. Space Phys. **115**, 09107 (2010). doi:10.1029/2009JA015140

J. Guo, X. Feng, B.A. Emery, J. Zhang, C. Xiang, F. Shen, W. Song, Energy transfer during intense geomagnetic storms driven by interplanetary coronal mass ejections and their sheath regions. J. Geophys. Res. Space Phys. **116**, 05106 (2011). doi:10.1029/2011JA016490

M.R. Hairston, K.A. Drake, R. Skoug, Saturation of the ionospheric polar cap potential during the October-November 2003 superstorms. J. Geophys. Res. Space Phys. **110**, 0926 (2005). doi:10.1029/2004JA010864

R. Hajra, E. Echer, B.T. Tsurutani, W.D. Gonzalez, Solar wind-magnetosphere energy coupling efficiency and partitioning: HILDCAAs and preceding CIR storms during solar cycle 23. J. Geophys. Res. Space Phys. **119**, 2675–2690 (2014). doi:10.1002/2013JA019646

R.A. Harrison, J.A. Davies, C. Möstl, Y. Liu, M. Temmer, M.M. Bisi, J.P. Eastwood, C.A. de Koning, N. Nitta, T. Rollett, C.J. Farrugia, R.J. Forsyth, B.V. Jackson, E.A. Jensen, E.K.J. Kilpua, D. Odstrcil, D.F. Webb, An analysis of the origin and propagation of the multiple coronal mass ejections of 2010 August 1. Astrophys. J. **750**, 45 (2012). doi:10.1088/0004-637X/750/1/45

H. Hasegawa, M. Fujimoto, T.-D. Phan, H. Rème, A. Balogh, M.W. Dunlop, C. Hashimoto, R. TanDokoro, Transport of solar wind into Earth's magnetosphere through rolled-up Kelvin-Helmholtz vortices. Nature **430**, 755–758 (2004). doi:10.1038/nature02799

T. Henke, J. Woch, R. Schwenn, U. Mall, G. Gloeckler, R. von Steiger, R.J. Forsyth, A. Balogh, Ionization state and magnetic topology of coronal mass ejections. J. Geophys. Res. **106**, 10597–10614 (2001). doi:10.1029/2000JA900176

H. Hietala, T.V. Laitinen, K. Andréeová, R. Vainio, A. Vaivads, M. Palmroth, T.I. Pulkkinen, H.E.J. Koskinen, E.A. Lucek, H. Rème, Supermagnetosonic jets behind a collisionless quasiparallel shock. Phys. Rev. Lett. **103**(24), 245001 (2009). doi:10.1103/PhysRevLett.103.245001

J. Hirshberg, A. Alksne, D.S. Colburn, S.J. Bame, A.J. Hundhausen, Observation of a solar flare induced interplanetary shock and helium-enriched driver gas. J. Geophys. Res. **75**, 1 (1970). doi:10.1029/JA075i001p00001

L. Holappa, K. Mursula, T. Asikainen, A new method to estimate annual solar wind parameters and contributions of different solar wind structures to geomagnetic activity. J. Geophys. Res. Space Phys. **119**, 9407–9418 (2014). doi:10.1002/2014JA020599

C.-S. Huang, G. Le, G.D. Reeves, Periodic magnetospheric substorms during fluctuating interplanetary magnetic field B_z. Geophys. Res. Lett. **31**, 14801 (2004). doi:10.1029/2004GL020180

K. Huttunen, H. Koskinen, Importance of post-shock streams and sheath region as drivers of intense magnetospheric storms and high-latitude activity. Ann. Geophys. **22**, 1729–1738 (2004). doi:10.5194/angeo-22-1729-2004

K.E.J. Huttunen, H.E.J. Koskinen, R. Schwenn, Variability of magnetospheric storms driven by different solar wind perturbations. J. Geophys. Res. Space Phys. **107**, 1121 (2002). doi:10.1029/2001JA900171

K.E.J. Huttunen, R. Schwenn, V. Bothmer, H.E.J. Koskinen, Properties and geoeffectiveness of magnetic clouds in the rising, maximum and early declining phases of solar cycle 23. Ann. Geophys. **23**, 625–641 (2005). doi:10.5194/angeo-23-625-2005

L. Jian, C.T. Russell, J.G. Luhmann, R.M. Skoug, Properties of interplanetary coronal mass ejections at one AU during 1995–2004. Sol. Phys. **239**, 393–436 (2006a)

L. Jian, C.T. Russell, J.G. Luhmann, R.M. Skoug, Properties of stream interactions at one AU during 1995–2004. Sol. Phys. **239**, 337–392 (2006b)

G.H. Jones, A. Balogh, Context and heliographic dependence of heliospheric planar magnetic structures. J. Geophys. Res. **105**, 12713–12724 (2000). doi:10.1029/2000JA900003

G.H. Jones, A. Rees, A. Balogh, R.J. Forsyth, The draping of heliospheric magnetic fields upstream of coronal mass ejecta. Geophys. Res. Lett. **29**, 1463 (2002). doi:10.1029/2001GL014110

V.K. Jordanova, H. Matsui, P.A. Puhl-Quinn, M.F. Thomsen, K. Mursula, L. Holappa, Ring current development during high speed streams. J. Atmos. Sol.-Terr. Phys. **71**, 1093–1102 (2009). doi:10.1016/j.jastp.2008.09.043

J.A. Joselyn, B.T. Tsurutani, Geomagnetic sudden impulses and storm sudden commencements—a note on terminology. EOS Trans. **71**, 1808 (1990). doi:10.1029/90EO00350

S. Jurac, J.C. Kasper, J.D. Richardson, A.J. Lazarus, Geomagnetic disturbances and their relationship to interplanetary shock parameters. Geophys. Res. Lett. **29**, 1463 (2002). doi:10.1029/2001GL014034

Y. Kamide, W. Baumjohann, I.A. Daglis, W.D. Gonzalez, M. Grande, J.A. Joselyn, R.L. McPherron, J.L. Phillips, E.G.D. Reeves, G. Rostoker, A.S. Sharma, H.J. Singer, B.T. Tsurutani, V.M. Vasyliunas, Current understanding of magnetic storms: storm-substorm relationships. J. Geophys. Res. **103** 17705–17728 (1998a)

Y. Kamide, J.-H. Shue, X. Li, G. Lu, M.J. Brittnacher, G.K. Parks, G.D. Reeves, Internally and externally triggered substorms: a case study of the January 10, 1997 events, in *Substorms-4*, 1998b

Y. Kamide, N. Yokoyama, W. Gonzalez, B.T. Tsurutani, I.A. Daglis, A. Brekke, S. Masuda, Two-step development of geomagnetic storms. J. Geophys. Res. **103**, 6917–6922 (1998c)

R. Kataoka, S. Watari, N. Shimada, H. Shimazu, K. Marubashi, Downstream structures of interplanetary fast shocks associated with coronal mass ejections. Geophys. Res. Lett. **32**, 12103 (2005). doi:10.1029/2005GL022777

R. Kataoka, D. Shiota, E. Kilpua, K. Keika, Pileup accident hypothesis of magnetic storm on 17 March 2015. Geophys. Res. Lett. **42**, 5155–5161 (2015). doi:10.1002/2015GL064816

E.K.J. Kilpua, J.G. Luhmann, J. Gosling, Y. Li, H. Elliott, C.T. Russell, L. Jian, A.B. Galvin, D. Larson, P. Schroeder, K. Simunac, G. Petrie, Small solar wind transients and their connection to the large-scale coronal structure. Sol. Phys. **256**, 327–344 (2009). doi:10.1007/s11207-009-9366-1

E.K.J. Kilpua, L.K. Jian, Y. Li, J.G. Luhmann, C.T. Russell, Multipoint ICME encounters: pre-STEREO and STEREO observations. J. Atmos. Sol.-Terr. Phys. **73**, 1228–1241 (2011). doi:10.1016/j.jastp.2010.10.012

E.K.J. Kilpua, Y. Li, J.G. Luhmann, L.K. Jian, C.T. Russell, On the relationship between magnetic cloud field polarity and geoeffectiveness. Ann. Geophys. **30**, 1037–1050 (2012). doi:10.5194/angeo-30-1037-2012

E.K.J. Kilpua, H. Hietala, H.E.J. Koskinen, D. Fontaine, L. Turc, Magnetic field and dynamic pressure ULF fluctuations in coronal-mass-ejection-driven sheath regions. Ann. Geophys. **31**, 1559–1567 (2013a)

E.K.J. Kilpua, A. Isavnin, A. Vourlidas, H.E.J. Koskinen, L. Rodriguez, On the relationship between interplanetary coronal mass ejections and magnetic clouds. Ann. Geophys. **31**, 1251–1265 (2013b)

E.K.J. Kilpua, E. Lumme, K. Andreeova, A. Isavnin, H.E.J. Koskinen, Properties and drivers of fast interplanetary shocks near the orbit of the Earth (1995–2013). J. Geophys. Res. **120**, 4112–4125 (2015a)

E.K.J. Kilpua, N. Olspert, A. Grigorievskiy, M.J. Käpylä, E.I. Tanskanen, H. Miyahara, R. Kataoka, J. Pelt, Y.D. Liu, Statistical study of strong and extreme geomagnetic disturbances and solar cycle characteristics. Astrophys. J. **806**, 272 (2015b)

E.K.J. Kilpua, H. Hietala, D.L. Turner, H.E.J. Koskinen, T.I. Pulkkinen, J.V. Rodriguez, G.D. Reeves, S.G. Claudepierre, H.E. Spence, Unraveling the drivers of the storm time radiation belt response. Geophys. Res. Lett. **42**, 3076–3084 (2015c)

E.K.J. Kilpua, H.E.J. Koskinen, T.I. Pulkkinen, Coronal mass ejections and their sheath regions in interplanetary space. Living Rev. Sol. Phys. (2017)

L.W. Klein, L.F. Burlaga, Interplanetary magnetic clouds at 1 AU. J. Geophys. Res. **87**, 613–624 (1982). doi:10.1029/JA087iA02p00613

A.J. Klimas, D.N. Baker, D.A. Roberts, D.H. Fairfield, J. Buechner, A nonlinear dynamical analogue model of geomagnetic activity. J. Geophys. Res. **97**, 12 (1992). doi:10.1029/92JA00794

D.J. Knipp, W.K. Tobiska, B.A. Emery, Direct and indirect thermospheric heating sources for solar cycles 21–23. Sol. Phys. **224**, 495–505 (2004). doi:10.1007/s11207-005-6393-4

H.E.J. Koskinen, *Physics of Space Storms: From the Solar Surface to the Earth* (Springer, Berlin, 2011)

H.E.J. Koskinen, E.I. Tanskanen, Magnetospheric energy budget and the epsilon parameter. J. Geophys. Res. Space Phys. **107**, 1415 (2002). doi:10.1029/2002JA009283

J.U. Kozyra, M.W. Liemohn, C.R. Clauer, A.J. Ridley, M.F. Thomsen, J.E. Borovsky, J.L. Roeder, V.K. Jordanova, W.D. Gonzalez, Multistep Dst development and ring current composition changes during the 4–6 June 1991 magnetic storm. J. Geophys. Res. Space Phys. **107**, 1224 (2002). doi:10.1029/2001JA000023

A.S. Krieger, A.F. Timothy, E.C. Roelof, A coronal hole and its identification as the source of a high velocity solar wind stream. Sol. Phys. **29**, 505–525 (1973). doi:10.1007/BF00150828

B. Lavraud, J.E. Borovsky, Altered solar wind-magnetosphere interaction at low Mach numbers: coronal mass ejections. J. Geophys. Res. Space Phys. **113**, 0008 (2008). doi:10.1029/2008JA013192

B. Lavraud, M.F. Thomsen, J.E. Borovsky, M.H. Denton, T.I. Pulkkinen, Magnetosphere preconditioning under northward IMF: evidence from the study of coronal mass ejection and corotating interaction region geoeffectiveness. J. Geophys. Res. Space Phys. **111**, 09208 (2006). doi:10.1029/2005JA011566

B. Lavraud, A. Ruffenach, A.P. Rouillard, P. Kajdic, W.B. Manchester, N. Lugaz, Geo-effectiveness and radial dependence of magnetic cloud erosion by magnetic reconnection. J. Geophys. Res. Space Phys. **119**, 26–35 (2014). doi:10.1002/2013JA019154

G.-M. Le, Z.-Y. Cai, H.-N. Wang, Z.-Q. Yin, P. Li, Solar cycle distribution of major geomagnetic storms. Res. Astron. Astrophys. **13**, 739–748 (2013). doi:10.1088/1674-4527/13/6/013

R.P. Lepping, L.F. Burlaga, J.A. Jones, Magnetic field structure of interplanetary magnetic clouds at 1 AU. J. Geophys. Res. **95**, 11957–11965 (1990). doi:10.1029/JA095iA08p11957

R.P. Lepping, L.F. Burlaga, A. Szabo, K.W. Ogilvie, W.H. Mish, D. Vassiliadis, A.J. Lazarus, J.T. Steinberg, C.J. Farrugia, L. Janoo, F. Mariani, The wind magnetic cloud and events of October 18-20, 1995: interplanetary properties and as triggers for geomagnetic activity. J. Geophys. Res. **102**, 14049–14064 (1997). doi:10.1029/97JA00272

Y. Li, J.G. Luhmann, B.J. Lynch, E.K.J. Kilpua, Cyclic reversal of magnetic cloud poloidal field. Sol. Phys. **270**, 331–346 (2011)

M.W. Liemohn, J.U. Kozyra, M.F. Thomsen, J.L. Roeder, G. Lu, J.E. Borovsky, T.E. Cayton, Dominant role of the asymmetric ring current in producing the stormtime Dst. J. Geophys. Res. **106**, 10883–10904 (2001). doi:10.1029/2000JA000326

M.W. Liemohn, M. Jazowski, J.U. Kozyra, N. Ganushkina, M.F. Thomsen, J.E. Borovsky, CIR versus CME drivers of the ring current during intense magnetic storms. Proc. R. Soc. Lond. Ser. A **466**, 3305–3328 (2010). doi:10.1098/rspa.2010.0075

F.A. Lindeman, Note on the theory of magnetic storms. Philos. Mag. **38**, 669–684 (1911)

Y. Liu, J.D. Richardson, J.W. Belcher, A statistical study of the properties of interplanetary coronal mass ejections from 0.3 to 5.4 AU. Planet. Space Sci. **53**, 3–17 (2005). doi:10.1016/j.pss.2004.09.023

Y. Liu, J.D. Richardson, J.W. Belcher, J.C. Kasper, R.M. Skoug, Plasma depletion and mirror waves ahead of interplanetary coronal mass ejections. J. Geophys. Res. Space Phys. **111**, 09108 (2006). doi:10.1029/2006JA011723

Y. Liu, J.G. Luhmann, R. Müller-Mellin, P.C. Schroeder, L. Wang, R.P. Lin, S.D. Bale, Y. Li, M.H. Acuña, J.-A. Sauvaud, A comprehensive view of the 2006 December 13 CME: from the Sun to interplanetary space. Astrophys. J. **689**, 563–571 (2008a). doi:10.1086/592031

Y. Liu, W.B. Manchester, J.D. Richardson, J.G. Luhmann, R.P. Lin, S.D. Bale, Deflection flows ahead of ICMEs as an indicator of curvature and geoeffectiveness. J. Geophys. Res. **113**, A00B03 (2008b)

Y.D. Liu, J.G. Luhmann, C. Möstl, J.C. Martinez-Oliveros, S.D. Bale, R.P. Lin, R.A. Harrison, M. Temmer, D.F. Webb, D. Odstrcil, Interactions between coronal mass ejections viewed in coordinated imaging and in situ observations. Astrophys. J. Lett. **746**, 15 (2012). doi:10.1088/2041-8205/746/2/L15

Y.D. Liu, J.G. Luhmann, N. Lugaz, C. Möstl, J.A. Davies, S.D. Bale, R.P. Lin, On Sun-to-Earth propagation of coronal mass ejections. Astrophys. J. **769**, 45 (2013). doi:10.1088/0004-637X/769/1/45

Y.D. Liu, J.G. Luhmann, P. Kajdič, E.K.J. Kilpua, N. Lugaz, N.V. Nitta, C. Möstl, B. Lavraud, S.D. Bale, C.J. Farrugia, A.B. Galvin, Observations of an extreme storm in interplanetary space caused by successive coronal mass ejections. Nat. Commun. **5**, 3481 (2014a)

Y.D. Liu, Z. Yang, R. Wang, J.G. Luhmann, J.D. Richardson, N. Lugaz, Sun-to-Earth characteristics of two coronal mass ejections interacting near 1 AU: formation of a complex ejecta and generation of a two-step geomagnetic storm. Astrophys. J. Lett. **793**, L41 2014b)

Y.D. Liu, H. Hu, R. Wang, Z. Yang, B. Zhu, Y.A. Liu, J.G. Luhmann, J.D. Richardson, Plasma and magnetic field characteristics of solar coronal mass ejections in relation to geomagnetic storm intensity and variability. Astrophys. J. Lett. **809**, 34 (2015). doi:10.1088/2041-8205/809/2/L34

Y.D. Liu, H. Hu, C. Wang, J.G. Luhmann, J.D. Richardson, Z. Yang, R. Wang, On sun-to-Earth propagation of coronal mass ejections: II. Slow events and comparison with others. Astrophys. J. Suppl. Ser. **222**, 23 (2016). doi:10.3847/0067-0049/222/2/23

M. Lockwood, M.J. Owens, L.A. Barnard, S. Bentley, C.J. Scott, C.E. Watt, On the origins and timescales of geoeffective IMF. Space Weather **14** 406–432 (2015). doi:10.1002/2016SW001375

R.E. Lopez, M. Wiltberger, S. Hernandez, J.G. Lyon, Solar wind density control of energy transfer to the magnetosphere. Geophys. Res. Lett. **31**, 08804 (2004). doi:10.1029/2003GL018780

R.E. Lopez, R. Bruntz, E.J. Mitchell, M. Wiltberger, J.G. Lyon, V.G. Merkin, Role of magnetosheath force balance in regulating the dayside reconnection potential. J. Geophys. Res. Space Phys. **115**, 12216 (2010). doi:10.1029/2009JA014597

E.A. Lucek, A. Balogh, The identification and characterization of Alfvénic fluctuations in ULYSSES data at midlatitudes. Astrophys. J. **507**, 984–990 (1998). doi:10.1086/306372

E.A. Lucek, T.S. Horbury, I. Dandouras, H. RèMe, Cluster observations of the Earth's quasi-parallel bow shock. J. Geophys. Res. Space Phys. **113**, 0702 (2008). doi:10.1029/2007JA012756

N. Lugaz, C.J. Farrugia, A new class of complex ejecta resulting from the interaction of two CMEs and its expected geoeffectiveness. Geophys. Res. Lett. **41**, 769–776 (2014). doi:10.1002/2013GL058789

N. Lugaz, C.J. Farrugia, C.W. Smith, K. Paulson, Shocks inside CMEs: a survey of properties from 1997 to 2006. J. Geophys. Res. Space Phys. **120**, 2409–2427 (2015). doi:10.1002/2014JA020848

N. Lugaz, C.J. Farrugia, C.-L. Huang, R.M. Winslow, H.E. Spence, N.A. Schwadron, Earth's magnetosphere and outer radiation belt under sub-Alfvénic solar wind. Nat. Commun. **7**, 13001 (2016)

L.R. Lyons, G.T. Blanchard, J.C. Samson, R.P. Lepping, T. Yamamoto, T. Moretto, Coordinated observations demonstrating external substorm triggering. J. Geophys. Res. **102**, 27039–27052 (1997). doi:10.1029/97JA02639

W. Manchester, E.K.J. Kilpua, Y.D. Liu, N. Lugaz, P. Riley, T. Török, B. Vršnak, The physical processes of CME/ICME evolution. Space Sci. Rev. (2017, this issue). doi:10.1007/s11214-017-0394-0. http://adsabs.harvard.edu/abs/2017SSRv..tmp...90M. Provided by the SAO/NASA Astrophysics Data System

E.W. Maunder, Magnetic disturbance and associated sun-spots. Mon. Not. R. Astron. Soc. **65**, 2 (1904). doi:10.1093/mnras/65.1.2

P.N. Mayaud, *Derivation, Meaning, and Use of Geomagnetic Indices*. Geophysical Monograph, vol. 22 (American Geophysical Union, Washington, 1980)

D.J. McComas, J.T. Gosling, S.J. Bame, E.J. Smith, H.V. Cane, A test of magnetic field draping induced BZ perturbations ahead of fast coronal mass ejecta. J. Geophys. Res. **94**, 1465–1471 (1989). doi:10.1029/JA094iA02p01465

R.L. McPherron, T. Terasawa, A. Nishida, Solar wind triggering of substorm expansion onset. J. Geomagn. Geoelectr. **38**, 1089–1108 (1986)

M.B. Moldwin, S. Ford, R. Lepping, J. Slavin, A. Szabo, Small-scale magnetic flux ropes in the solar wind. Geophys. Res. Lett. **27**, 57–60 (2000). doi:10.1029/1999GL010724

S.K. Morley, M.P. Freeman, On the association between northward turnings of the interplanetary magnetic field and substorm onsets. Geophys. Res. Lett. **34**, 08104 (2007). doi:10.1029/2006GL028891

P. Morrison, Solar origin of cosmic-ray time variations. Phys. Rev. **101**, 1397–1404 (1956). doi:10.1103/PhysRev.101.1397

C. Möstl, C.J. Farrugia, E.K.J. Kilpua, L.K. Jian, Y. Liu, J.P. Eastwood, R.A. Harrison, D.F. Webb, M. Temmer, D. Odstrcil, J.A. Davies, T. Rollett, J.G. Luhmann, N. Nitta, T. Mulligan, E.A. Jensen, R. Forsyth, B. Lavraud, C.A. de Koning, A.M. Veronig, A.B. Galvin, T.L. Zhang, B.J. Anderson, Multi-point shock and flux rope analysis of multiple interplanetary coronal mass ejections around 2010 August 1 in the inner heliosphere. Astrophys. J. **758**, 10 (2012). doi:10.1088/0004-637X/758/1/10

T. Mulligan, C.T. Russell, J.G. Luhmann, Solar cycle evolution of the structure of magnetic clouds in the inner heliosphere. Geophys. Res. Lett. **25**, 2959–2962 (1998). doi:10.1029/98GL01302

M. Myllys, N. Partamies, L. Juusola, Latitude dependence of long-term geomagnetic activity and its solar wind drivers. Ann. Geophys. **33**, 573–581 (2015). doi:10.5194/angeo-33-573-2015

M. Myllys, E.K.J. Kilpua, B. Lavraud, T.I. Pulkkinen, Solar wind-magnetosphere coupling efficiency during ejecta and sheath-driven geomagnetic storms. J. Geophys. Res. Space Phys. **121**, 4378–4396 (2016). doi:10.1002/2016JA022407

M. Myllys, E.K.J. Kipua, B. Lavraud, Interplay of solar wind parameters and physical mechanisms producing the saturation of the cross polar cap potential. Geophys. Res. Lett. **44**, 3019–3027 (2017). doi:10.1002/2017GL072676

P.T. Newell, K. Liou, Solar wind driving and substorm triggering. J. Geophys. Res. Space Phys. **116**, 03229 (2011). doi:10.1029/2010JA016139

P.T. Newell, T. Sotirelis, K. Liou, C.-I. Meng, F.J. Rich, A nearly universal solar wind-magnetosphere coupling function inferred from 10 magnetospheric state variables. J. Geophys. Res. Space Phys. **112**, 01206 (2007). doi:10.1029/2006JA012015

H.W. Newton, A.S. Milsom, The distribution of great and small geomagnetic storms in the sunspot cycle. J. Geophys. Res. **59**, 203–214 (1954). doi:10.1029/JZ059i002p00203

N.S. Nikolaeva, Y.I. Yermolaev, I.G. Lodkina, Dependence of geomagnetic activity during magnetic storms on the solar wind parameters for different types of streams. Geomagn. Aeron. **51**, 49–65 (2011). doi:10.1134/S0016793211010099

J.T. Nolte, A.S. Krieger, A.F. Timothy, R.E. Gold, E.C. Roelof, G. Vaiana, A.J. Lazarus, J.D. Sullivan, P.S. McIntosh, Coronal holes as sources of solar wind. Sol. Phys. **46**, 303–322 (1976). doi:10.1007/BF00149859

T.P. O'Brien, R.L. McPherron, An empirical phase space analysis of ring current dynamics: solar wind control of injection and decay. J. Geophys. Res. **105**, 7707–7720 (2000). doi:10.1029/1998JA000437

D.M. Oliveira, J. Raeder, Impact angle control of interplanetary shock geoeffectiveness. J. Geophys. Res. Space Phys. **119**, 8188–8201 (2014). doi:10.1002/2014JA020275

D.M. Oliveira, J. Raeder, Impact angle control of interplanetary shock geoeffectiveness: a statistical study. J. Geophys. Res. Space Phys. **120**, 4313–4323 (2015). doi:10.1002/2015JA021147

N. Omidi, H. Zhang, D. Sibeck, D. Turner, Spontaneous hot flow anomalies at quasi-parallel shocks: 2. Hybrid simulations. J. Geophys. Res. Space Phys. **118**, 173–180 (2013). doi:10.1029/2012JA018099

A. Osmane, A.P. Dimmock, R. Naderpour, T.I. Pulkkinen, K. Nykyri, The impact of solar wind ULF B_z fluctuations on geomagnetic activity for viscous timescales during strongly northward and southward IMF. J. Geophys. Res. Space Phys. **120**, 9307–9322 (2015). doi:10.1002/2015JA021505

M.J. Owens, P.J. Cargill, C. Pagel, G.L. Siscoe, N.U. Crooker, Characteristic magnetic field and speed properties of interplanetary coronal mass ejections and their sheath regions. J. Geophys. Res. Space Phys. **110**, 01105 (2005). doi:10.1029/2004JA010814

E. Palmerio, E.K.J. Kilpua, N.P. Savani, Planar magnetic structures in coronal mass ejection-driven sheath regions. Ann. Geophys. **34**, 313–322 (2016). doi:10.5194/angeo-34-313-2016

M. Palmroth, T.I. Pulkkinen, P. Janhunen, D.J. McComas, C.W. Smith, H.E.J. Koskinen, Role of solar wind dynamic pressure in driving ionospheric Joule heating. J. Geophys. Res. Space Phys. **109**, 11302 (2004). doi:10.1029/2004JA010529

M. Palmroth, H.E.J. Koskinen, T.I. Pulkkinen, P.K. Toivanen, P. Janhunen, S.E. Milan, M. Lester, Magnetospheric feedback in solar wind energy transfer. J. Geophys. Res. Space Phys. **115**, 0010 (2010). doi:10.1029/2010JA015746

W. Park, J. Lee, Y. Yi, N. Ssessanga, S. Oh, Storm sudden commencements without interplanetary shocks. J. Astron. Space Sci. **32**, 181–187 (2015). doi:10.5140/JASS.2015.32.3.181

J.H. Piddington, Interplanetary magnetic field and its control of cosmic-ray variations. Phys. Rev. **112**, 589–596 (1958). doi:10.1103/PhysRev.112.589

T. Pulkkinen, Space weather: terrestrial perspective. Living Rev. Sol. Phys. **4**, 1 (2007). doi:10.12942/lrsp-2007-1

T.I. Pulkkinen, A.P. Dimmock, A. Osmane, K. Nykyri, Solar wind energy input to the magnetosheath and at the magnetopause. Geophys. Res. Lett. **42**, 4723–4730 (2015). doi:10.1002/2015GL064226

J. Raeder, G. Lu, Polar cap potential saturation during large geomagnetic storms. Adv. Space Res. **36**, 1804–1808 (2005). doi:10.1016/j.asr.2004.05.010

P.H. Reiff, R.W. Spiro, T.W. Hill, Dependence of polar cap potential drop on interplanetary parameters. J. Geophys. Res. **86**, 7639–7648 (1981). doi:10.1029/JA086iA09p07639

I.G. Richardson, H.V. Cane, Near-Earth interplanetary coronal mass ejections during solar cycle 23 (1996–2009): catalog and summary of properties. Sol. Phys. **264**, 189–237 (2010). doi:10.1007/s11207-010-9568-6

I.G. Richardson, H.V. Cane, Solar wind drivers of geomagnetic storms during more than four solar cycles. J. Space Weather Space Clim. **2**(27), 01 (2012). doi:10.1051/swsc/2012001

I.G. Richardson, D.F. Webb, J. Zhang, D.B. Berdichevsky, D.A. Biesecker, J.C. Kasper, R. Kataoka, J.T. Steinberg, B.J. Thompson, C.-C. Wu, A.N. Zhukov, Major geomagnetic storms (Dst ≤ −100 nT) generated by corotating interaction regions. J. Geophys. Res. Space Phys. **111**, 0709 (2006). doi:10.1029/2005JA011476

P. Riley, R.M. Caplan, J. Giacalone, D. Lario, Y. Liu, Properties of the fast forward shock driven by the July 23 2012 extreme coronal mass ejection. Astrophys. J. **819**, 57 (2016). doi:10.3847/0004-637X/819/1/57

A.P. Rouillard, N.R. Sheeley Jr., T.J. Cooper, J.A. Davies, B. Lavraud, E.K.J. Kilpua, R.M. Skoug, J.T. Steinberg, A. Szabo, A. Opitz, J.-A. Sauvaud, The solar origin of small interplanetary transients. Astrophys. J. **734**, 7 (2011). doi:10.1088/0004-637X/734/1/7

A. Ruffenach, B. Lavraud, C.J. Farrugia, P. Démoulin, S. Dasso, M.J. Owens, J.-A. Sauvaud, A.P. Rouillard, A. Lynnyk, C. Foullon, N.P. Savani, J.G. Luhmann, A.B. Galvin, Statistical study of magnetic cloud erosion by magnetic reconnection. J. Geophys. Res. Space Phys. **120**, 43–60 (2015). doi:10.1002/2014JA020628

C.T. Russell, R.L. McPherron, Semiannual variation of geomagnetic activity. J. Geophys. Res. **78**, 92 (1973). doi:10.1029/JA078i001p00092

C.T. Russell, L.K. Jian, X. Blanco-Cano, J.G. Luhmann, STEREO observations of upstream and downstream waves at low Mach number shocks. Geophys. Res. Lett. **36**, 03106 (2009). doi:10.1029/2008GL036991

C.T. Russell, R.A. Mewaldt, J.G. Luhmann, G.M. Mason, T.T. von Rosenvinge, C.M.S. Cohen, R.A. Leske, R. Gomez-Herrero, A. Klassen, A.B. Galvin, K.D.C. Simunac, The very unusual interplanetary coronal mass ejection of 2012 July 23: a blast wave mediated by solar energetic particles. Astrophys. J. **770**, 38 (2013). doi:10.1088/0004-637X/770/1/38

T. Saemundsson, Statistics of geomagnetic storms and solar activity. Mon. Not. R. Astron. Soc. **123**, 299 (1962). doi:10.1093/mnras/123.4.299

M.D. Salas, The curious events leading to the theory of shock waves. Shock Waves **16**, 477–487 (2007). doi:10.1007/s00193-007-0084-z

A.A. Samsonov, D.G. Sibeck, J. Imber, MHD simulation for the interaction of an interplanetary shock with the Earth's magnetosphere. J. Geophys. Res. Space Phys. **112**, 12220 (2007). doi:10.1029/2007JA012627

A.A. Samsonov, V.A. Sergeev, M.M. Kuznetsova, D.G. Sibeck, Asymmetric magnetospheric compressions and expansions in response to impact of inclined interplanetary shock. Geophys. Res. Lett. **42**, 4716–4722 (2015). doi:10.1002/2015GL064294

R. Schwenn, Direct correlations between coronal transients and interplanetary disturbances. Space Sci. Rev. **34**, 85–99 (1983). doi:10.1007/BF00221199

R. Schwenn, A. dal Lago, E. Huttunen, W.D. Gonzalez, The association of coronal mass ejections with their effects near the Earth. Ann. Geophys. **23**, 1033–1059 (2005). doi:10.5194/angeo-23-1033-2005

V.A. Sergeev, R.J. Pellinen, T.I. Pulkkinen, Steady magnetospheric convection: a review of recent results. Space Sci. Rev. **75**, 551–604 (1996). doi:10.1007/BF00833344

N.R. Sheeley Jr., A.P. Rouillard, Tracking streamer blobs into the heliosphere. Astrophys. J. **715**, 300–309 (2010). doi:10.1088/0004-637X/715/1/300

N.R. Sheeley Jr., R.A. Howard, D.J. Michels, M.J. Koomen, R. Schwenn, K.H. Muehlhaeuser, H. Rosenbauer, Coronal mass ejections and interplanetary shocks. J. Geophys. Res. **90**, 163–175 (1985). doi:10.1029/JA090iA01p00163

N.R. Sheeley, Y.-M. Wang, S.H. Hawley, G.E. Brueckner, K.P. Dere, R.A. Howard, M.J. Koomen, C.M. Korendyke, D.J. Michels, S.E. Paswaters, D.G. Socker, O.C. St. Cyr, D. Wang, P.L. Lamy, A. Llebaria, R. Schwenn, G.M. Simnett, S. Plunkett, D.A. Biesecker, Measurements of flow speeds in the corona between 2 and 30 $R_\odot$. Astrophys. J. **484**, 472–478 (1997)

J.-H. Shue, P. Song, C.T. Russell, J.T. Steinberg, J.K. Chao, G. Zastenker, O.L. Vaisberg, S. Kokubun, H.J. Singer, T.R. Detman, H. Kawano, Magnetopause location under extreme solar wind conditions. J. Geophys. Res. **103**, 17691–17700 (1998). doi:10.1029/98JA01103

G. Siscoe, D. Odstrcil, Ways in which ICME sheaths differ from magnetosheaths. J. Geophys. Res. Space Phys. **113**, 0007 (2008). doi:10.1029/2008JA013142

G. Siscoe, P.J. MacNeice, D. Odstrcil, East-West asymmetry in coronal mass ejection geoeffectiveness. Space Weather **5**, 04002 (2007). doi:10.1029/2006SW000286

E.J. Smith, J.A. Slavin, R.D. Zwickl, S.J. Bame, Shocks and storm sudden commencements, in *Solar Wind Magnetosphere Coupling*, ed. by Y. Kamide, J.A. Slavin. Astrophysics and Space Science Library, vol. 126 (1986), pp. 345–365

K. Snekvik, E.I. Tanskanen, E.K.J. Kilpua, An automated identification method for Alfvénic streams and their geoeffectiveness. J. Geophys. Res. Space Phys. **118**, 5986–5998 (2013). doi:10.1002/jgra.50588

C.P. Sonett, D.S. Colburn, L. Davis, E.J. Smith, P.J. Coleman, Evidence for a collision-free magnetohydrodynamic shock in interplanetary space. Phys. Rev. Lett. **13**, 153–156 (1964). doi:10.1103/PhysRevLett.13.153

P. Subramanian, K.P. Dere, Source regions of coronal mass ejections. Astrophys. J. **561**, 372–395 (2001). doi:10.1086/323213

E.I. Tanskanen, J.A. Slavin, A.J. Tanskanen, A. Viljanen, T.I. Pulkkinen, H.E.J. Koskinen, A. Pulkkinen, J. Eastwood, Magnetospheric substorms are strongly modulated by interplanetary high-speed streams. Geophys. Res. Lett. **32**, 16104 (2005). doi:10.1029/2005GL023318

M. Temmer, N.V. Nitta, Interplanetary propagation behavior of the fast coronal mass ejection on 23 July 2012. Sol. Phys. **290**, 919–932 (2015). doi:10.1007/s11207-014-0642-3

T. Terasawa, M. Fujimoto, T. Mukai, I. Shinohara, Y. Saito, T. Yamamoto, S. Machida, S. Kokubun, A.J. Lazarus, J.T. Steinberg, R.P. Lepping, Solar wind control of density and temperature in the near-Earth plasma sheet: WIND/GEOTAIL collaboration. Geophys. Res. Lett. **24**, 935–938 (1997). doi:10.1029/96GL04018

K. Toman, Identification of M-regions on the Sun. Nature **181**, 641–642 (1958). doi:10.1038/181641a0

S. Tomczyk, S.W. McIntosh, Time-distance seismology of the solar corona with CoMP. Astrophys. J. **697**, 1384–1391 (2009). doi:10.1088/0004-637X/697/2/1384

R. Tousey, The solar corona, in *Space Research Conference*, ed. by M.J. Rycroft, S.K. Runcorn. Space Research Conference, vol. 2 (1973), pp. 713–730

R.A. Treumann, Fundamentals of collisionless shocks for astrophysical application, 1. Non-relativistic shocks. Astron. Astrophys. Rev. **17**, 409–535 (2009). doi:10.1007/s00159-009-0024-2

B.T. Tsurutani, W.D. Gonzalez, The cause of high-intensity long-duration continuous AE activity (HILDCAAS)—interplanetary Alfven wave trains. Planet. Space Sci. **35**, 405–412 (1987). doi:10.1016/0032-0633(87)90097-3

B.T. Tsurutani, E.J. Smith, W.D. Gonzalez, F. Tang, S.I. Akasofu, Origin of interplanetary southward magnetic fields responsible for major magnetic storms near solar maximum (1978–1979). J. Geophys. Res. **93**, 8519–8531 (1988). doi:10.1029/JA093iA08p08519

B.T. Tsurutani, Y.T. Lee, W.D. Gonzalez, F. Tang, Great magnetic storms. Geophys. Res. Lett. **19**, 73–76 (1992). doi:10.1029/91GL02783

B.T. Tsurutani, W.D. Gonzalez, A.L.C. Gonzalez, F. Tang, J.K. Arballo, M. Okada, Interplanetary origin of geomagnetic activity in the declining phase of the solar cycle. J. Geophys. Res. **100**, 21717–21734 (1995). doi:10.1029/95JA01476

B.T. Tsurutani, X.-Y. Zhou, W.D. Gonzalez, A lack of substorm expansion phases during magnetic storms induced by magnetic clouds, in *Disturbances in Geospace: The Storm-Substorm Relationship*, ed. by A. Surjalal Sharma, Y. Kamide, G.S. Lakhina. Washington DC American Geophysical Union Geophysical Monograph Series, vol. 142 (2003), p. 23. doi:10.1029/142GM03

B.T. Tsurutani, W.D. Gonzalez, X.-Y. Zhou, R.P. Lepping, V. Bothmer, Properties of slow magnetic clouds. J. Atmos. Sol.-Terr. Phys. **66**, 147–151 (2004). doi:10.1016/j.jastp.2003.09.007

B.T. Tsurutani, W.D. Gonzalez, A.L.C. Gonzalez, F.L. Guarnieri, N. Gopalswamy, M. Grande, Y. Kamide, Y. Kasahara, G. Lu, I. Mann, R. McPherron, F. Soraas, V. Vasyliunas, Corotating solar wind streams and recurrent geomagnetic activity: a review. J. Geophys. Res. Space Phys. **111**, 0701 (2006). doi:10.1029/2005JA011273

B.T. Tsurutani, R. Hajra, E. Echer, J.W. Gjerloev, Extremely intense (SML ≤ −2500 nT) substorms: isolated events that are externally triggered? Ann. Geophys. **33**, 519–524 (2015). doi:10.5194/angeo-33-519-2015

L. Turc, D. Fontaine, P. Savoini, R. Modolo, 3D hybrid simulations of the interaction of a magnetic cloud with a bow shock. J. Geophys. Res. Space Phys. **120**, 6133–6151 (2015). doi:10.1002/2015JA021318

L. Turc, C.P. Escoubet, D. Fontaine, E.K.J. Kilpua, S. Enestam, Cone angle control of the interaction of magnetic clouds with the Earth's bow shock. Geophys. Res. Lett. **43**, 4781–4789 (2016). doi:10.1002/2016GL068818

N.E. Turner, E.J. Mitchell, D.J. Knipp, B.A. Emery, Energetics of magnetic storms driven by corotating interaction regions: a study of geoeffectiveness, in *Recurrent Magnetic Storms: Corotating Solar Wind*, ed. by R. McPherron, W. Gonzalez, G. Lu, H.A. José, S. Natchimuthukonar Gopalswamy. Geophysical Monograph Series, vol. 167 (2006, American Geophysical Union, Washington), p. 113. doi:10.1029/167GM11

N.E. Turner, W.D. Cramer, S.K. Earles, B.A. Emery, Geoefficiency and energy partitioning in CIR-driven and CME-driven storms. J. Atmos. Sol.-Terr. Phys. **71**, 1023–1031 (2009). doi:10.1016/j.jastp.2009.02.005

M. Vandas, S. Fischer, M. Dryer, Z. Smith, T. Detman, A. Geranios, MHD simulation of an interaction of a shock wave with a magnetic cloud. J. Geophys. Res. **102**, 22295–22300 (1997). doi:10.1029/97JA01675

V.M. Vasyliunas, Theoretical models of magnetic field line merging. I. Rev. Geophys. Space Phys. **13**, 303–336 (1975). doi:10.1029/RG013i001p00303

R. von Steiger, Space physics—grand challenges for the 21st century. Front. Phys. **1**, 6 (2013). doi:10.3389/fphy.2013.00006

R. von Steiger, T.H. Zurbuchen, A. Kilchenmann, Latitude distribution of interplanetary coronal mass ejections during solar maximum, in *Solar Wind 11/SOHO 16, Connecting Sun and Heliosphere*, ed. by B. Fleck, T.H. Zurbuchen, H. Lacoste. ESA Special Publication, vol. 592 (2005), p. 317

M.-T. Walach, S.E. Milan, Are steady magnetospheric convection events prolonged substorms? J. Geophys. Res. Space Phys. **120**, 1751–1758 (2015). doi:10.1002/2014JA020631

B.M. Walsh, D.G. Sibeck, Y. Wang, D.H. Fairfield, Dawn-dusk asymmetries in the Earth's magnetosheath. J. Geophys. Res. Space Phys. **117**, 12211 (2012). doi:10.1029/2012JA018240

Y.M. Wang, P.Z. Ye, S. Wang, G.P. Zhou, J.X. Wang, A statistical study on the geoeffectiveness of Earth-directed coronal mass ejections from March 1997 to December 2000. J. Geophys. Res. Space Phys. **107**, 1340 (2002). doi:10.1029/2002JA009244

Y.M. Wang, P.Z. Ye, S. Wang, Multiple magnetic clouds: several examples during March–April 2001. J. Geophys. Res. Space Phys. **108**, 1370 (2003). doi:10.1029/2003JA009850

Y.-M. Wang, N.R. Sheeley Jr., N.B. Rich, Coronal pseudostreamers. Astrophys. J. **658**, 1340–1348 (2007). doi:10.1086/511416

C. Wang, J.B. Liu, H. Li, Z.H. Huang, J.D. Richardson, J.R. Kan, Geospace magnetic field responses to interplanetary shocks. J. Geophys. Res. Space Phys. **114**, 05211 (2009). doi:10.1029/2008JA013794

Y. Wang, Q. Zhang, J. Liu, C. Shen, F. Shen, Z. Yang, T. Zic, B. Vrsnak, D.F. Webb, R. Liu, S. Wang, J. Zhang, Q. Hu, B. Zhuang, On the propagation of a geoeffective coronal mass ejection during 15–17 March 2015. J. Geophys. Res. Space Phys. **121**, 7423–7434 (2016). doi:10.1002/2016JA022924

D.F. Webb, T.A. Howard, Coronal mass ejections: observations. Living Rev. Sol. Phys. **9**, 3 (2012). doi:10.1007/lrsp-2012-3. http://www.livingreviews.org/lrsp-2012-3

D.F. Webb, E.W. Cliver, N.U. Crooker, O.C.S. Cry, B.J. Thompson, Relationship of halo coronal mass ejections, magnetic clouds, and magnetic storms. J. Geophys. Res. **105**, 7491–7508 (2000). doi:10.1029/1999JA000275

D.F. Webb, C. Möstl, B.V. Jackson, M.M. Bisi, T.A. Howard, T. Mulligan, E.A. Jensen, L.K. Jian, J.A. Davies, C.A. de Koning, Y. Liu, M. Temmer, J.M. Clover, C.J. Farrugia, R.A. Harrison, N. Nitta, D. Odstrcil, S.J. Tappin, H.-S. Yu, Heliospheric imaging of 3D density structures during the multiple coronal mass ejections of late July to early August 2010. Sol. Phys. **285**, 317–348 (2013). doi:10.1007/s11207-013-0260-5

R.F. Wimmer-Schweingruber, R. von Steiger, R. Paerli, Solar wind stream interfaces in corotating interaction regions: SWICS/Ulysses results. J. Geophys. Res. **102**, 17407–17418 (1997). doi:10.1029/97JA00951

R.F. Wimmer-Schweingruber, N.U. Crooker, A. Balogh, V. Bothmer, R.J. Forsyth, P. Gazis, J.T. Gosling, T. Horbury, A. Kilchenmann, I.G. Richardson, J.D. Richardson, P. Riley, L. Rodriguez, R.V. Steiger, P. Wurz, T.H. Zurbuchen, Understanding interplanetary coronal mass ejection signatures. Space Sci. Rev. **123**, 177–216 (2006). doi:10.1007/s11214-006-9017-x. Report of Working Group B

Y.Q. Xie, P.B. Zuo, X.S. Feng, Y. Zhang, Properties of solar wind dynamic pressure pulses at 1 AU during the deep minimum between solar cycles 23 and 24. Sol. Phys. **290**, 1835–1849 (2015). doi:10.1007/s11207-015-0700-5

Y.I. Yermolaev, N.S. Nikolaeva, I.G. Lodkina, M.Y. Yermolaev, Specific interplanetary conditions for CIR-, sheath-, and ICME-induced geomagnetic storms obtained by double superposed epoch analysis. Ann. Geophys. **28**, 2177–2186 (2010). doi:10.5194/angeo-28-2177-2010

W. Yu, C.J. Farrugia, N. Lugaz, A.B. Galvin, E.K.J. Kilpua, H. Kucharek, C. Möstl, M. Leitner, R.B. Torbert, K.D.C. Simunac, J.G. Luhmann, A. Szabo, L.B. Wilson, K.W. Ogilvie, J.-A. Sauvaud, A statistical analysis of properties of small transients in the solar wind 2007-2009: STEREO and wind observations. J. Geophys. Res. Space Phys. **119**, 689–708 (2014). doi:10.1002/2013JA019115

R. Zelwer, P.C.B. Fernando, S.H. Ward, Interplanetary magnetic field data and corresponding geomagnetic effects for the storm of October 7, 1962. J. Geophys. Res. **72**, 3471–3482 (1967). doi:10.1029/JZ072i013p03471

J. Zhang, I.G. Richardson, D.F. Webb, N. Gopalswamy, E. Huttunen, J.C. Kasper, N.V. Nitta, W. Poomvises, B.J. Thompson, C.-C. Wu, S. Yashiro, A.N. Zhukov, Solar and interplanetary sources of major geomagnetic storms (Dst ≤ -100 nT) during 1996–2005. J. Geophys. Res. Space Phys. **112**, 10102 (2007). doi:10.1029/2007JA012321

Y. Zhang, W. Sun, X.S. Feng, C.S. Deehr, C.D. Fry, M. Dryer, Statistical analysis of corotating interaction regions and their geoeffectiveness during solar cycle 23. J. Geophys. Res. Space Phys. **113**, 08106 (2008). doi:10.1029/2008JA013095

H. Zhang, D.G. Sibeck, Q.-G. Zong, N. Omidi, D. Turner, L.B.N. Clausen, Spontaneous hot flow anomalies at quasi-parallel shocks: 1. observations. J. Geophys. Res. Space Phys. **118**, 3357–3363 (2013). doi:10.1002/jgra.50376

J.J. Zhang, C. Wang, T.R. Sun, C.M. Liu, K.R. Wang, GIC due to storm sudden commencement in low-latitude high-voltage power network in China: observation and simulation. Space Weather **13**, 643–655 (2015). doi:10.1002/2015SW001263

L. Zhao, T.H. Zurbuchen, L.A. Fisk, Global distribution of the solar wind during solar cycle 23: ACE observations. Geophys. Res. Lett. **36**, 14104 (2009). doi:10.1029/2009GL039181

P. Zuo, X. Feng, Y. Xie, Y. Wang, X. Xu, A statistical survey of dynamic pressure pulses in the solar wind based on WIND observations. Astrophys. J. **808**, 83 (2015). doi:10.1088/0004-637X/808/1/83

T.H. Zurbuchen, I.G. Richardson, In-situ solar wind and magnetic field signatures of interplanetary coronal mass ejections. Space Sci. Rev. **123**, 31–43 (2006). doi:10.1007/s11214-006-9010-4